Supporting Information

Achieving Submicrosecond Thermally Activated Delayed Fluorescence Lifetime and Highly Efficient Electroluminescence by Fine Tuning of Phenoxazine-Pyrimidine Structure

Tomas Serevičius[a]*, Rokas Skaisgiris[a], Jelena Dodonova[b], Laimis Jagintavičius[b], Dovydas Banevičius[a], Karolis Kazlauskas[a], Sigitas Tumkevičius[b], Saulius Juršėnas[a]

[a]Institute of Photonics and Nanotechnology, Vilnius University, Sauletekio 3, LT-10257 Vilnius, Lithuania.

[b]Institute of Chemistry, Vilnius University, Naugarduko 24, LT-03225, Vilnius, Lithuania.

*Corresponding author: tomas.serevicius@tmi.vu.lt

Table of Contents

Synthesis and characterization data of compounds.

Synthesis of 10-(4-(4,4,5,5-tetramethyl-1,3,2-dioxaborolan-2-yl)phenyl)-10*H*-phenoxazines (1a,b) and boronic acid 2.

Compounds **1a,b** and **2** were synthesized starting with phenoxazine and corresponding p-bromoiodobenzenes **5a-c** in two steps according to the scheme S1.

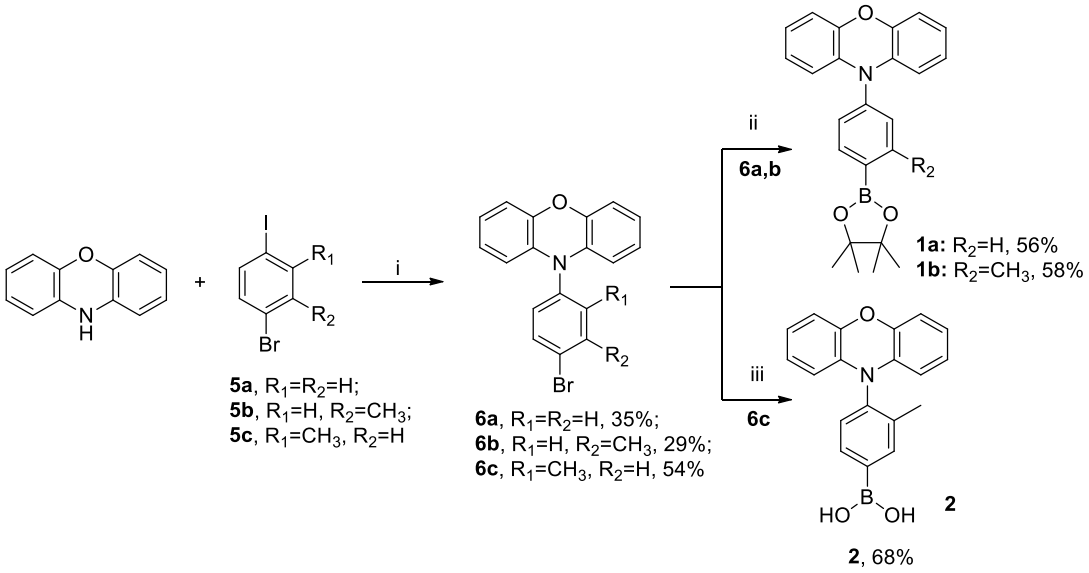

Scheme S1. *Reagents and conditions*: i) **1a**, **b** or **c** (1.5 equiv.), $Pd(OAc)_2$ (5 mol%), P(*t*-Bu)$_3$·HBF_4 (10 mol%), NaO*t*-Bu (3 equiv.), toluene, Ar, rt, 2-6 h; ii) B_2Pin_2 (1.3 equiv.), $PdCl_2(dppf)*CH_2Cl_2$ (10 mol%), KOAc (5 equiv.), dioxane, Ar, 110 °C, 24 h; iii) *n*-BuLi (1.8 equiv.), THF, Ar, -78 ºC, 1 h; then $B(OCH_3)_3$ (2.5 equiv.), - 78 °C to rt, 24 h.; then 1M HCl, rt, 1 h.

Synthesis of 10-(4-bromophenyl)-10*H*-phenoxazines (6a-c). General procedure.

Phenoxazine (**PXZ**) (1 g, 5.5 mmol), $Pd(OAc)_2$ (0.061 g, 0.275 mmol, 5 mol %), P(*t*-Bu)3·HBF4 (0.16 g, 0.546 mmol, 10 mol %), corresponding bromoiodobenzene **5a-c** (1.5 equiv., 8.25 mmol), NaO*t*-Bu (3 equiv., 1.57 g, 16.5 mmol) and toluene (25 mL) were placed in an Erlenmeyer flask equipped with a magnetic stir bar. The flask was purged with argon and the reaction mixture was stirred vigorously at room temperature for 2-6 h. After completion of the reaction, toluene was removed by distillation under reduced pressure. Water (50 mL) was added and the aqueous solution was extracted with chloroform (4×50 mL). The combined extract was dried with anhydrous Na_2SO_4, filtered and chloroform was removed by distillation under reduced pressure. Residue was purified by column chromatography using chloroform:petroleum ether (1:9) as an eluent.

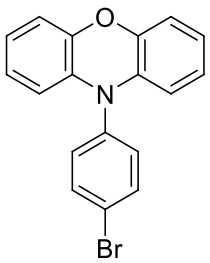

Figure S1. Molecular structure of 10-(4-bromophenyl)-10*H*-phenoxazine **(6a).**

White solid (0.66 g, 35%), mp 200-201 °C. ^{1}H NMR (400 MHz, $CDCl_3$) δ (ppm): 5.94 (2H, d, *J* = 8 Hz, phenoxazine-1,9-H), 6.61-6.73 (6H, m, phenoxazine-2-4,6-8-H), 7.27 (2H, d, *J* = 8 Hz, Ph-2,6-H), 7.75 (2H, d, *J* = 8 Hz, Ph-3,5-H).
NMR spectra and melting point of compound **6a** match with those described in ref[1].

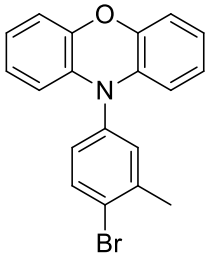

Figure S2. Molecular structure of 10-(4-bromo-3-methylphenyl)-10*H*-phenoxazine **(6b)**.

White solid (0.57 g, 29%), mp 164 °C. ^{1}H NMR (400 MHz, $CDCl_3$) δ (ppm): 2.48 (3H, s, CH_3); 5.95 (2H, d, *J* = 7.6 Hz, phenoxazine-1,9-H); 6.60 – 6.73 (6H, m, phenoxazine-2-4,6-8-H); 7.08 (1H, dd, *J* = 8.3 Hz, *J* = 2.4 Hz, Ph-6-H); 7.26 (1H, d, *J* = 2.4 Hz, Ph-2-H); 7.78 (1H, d, *J* = 8.3 Hz, Ph-5- H). ^{13}C NMR (100 MHz, $CDCl_3$) δ (ppm): 23.1; 113.2; 115.5; 121.5; 123.3; 124.8; 129.7; 133.0; 134.1; 135.0; 138.1; 141.3; 143.9. HRMS-ESI: m/z calcd. for $[M]^+$ ($C_{19}H_{14}BrNO$): 351.0253, found: 351.0253.

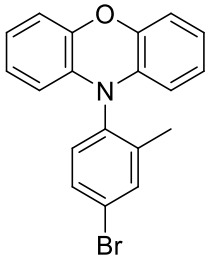

Figure S3. Molecular structure of 10-(4-bromo-2-methylphenyl)-10*H*-phenoxazine **(6c).**

White solid (1.0 g, 54%), mp 128 °C. ^{1}H NMR (400 MHz, $CDCl_3$) δ (ppm): 2.25 (3H, s, CH_3); 5.81 (2H, dd, *J* = 7.7 Hz, *J* = 1.4 Hz, phenoxazine-1,9-H), 6.60 – 6.73 (6H, m, phenoxazine-2-4,6-8-H), 7.18 (1H, d, *J* = 8.3 Hz, Ph-6-H), 7.56 (1H, dd, *J* = 8.3 Hz, *J* = 2.0 Hz, Ph-5-H), 7.64 (1H, d, *J* = 2.0 Hz, Ph-3-H). ^{13}C NMR (100 MHz, $CDCl_3$) δ (ppm): 17.5, 112.5, 115.6, 121.5, 122.6, 123.5, 131.9, 132.8, 133.0, 135.3, 136.0, 141.5, 143.8. HRMS-ESI: m/z calcd. for $[M]^+$ ($C_{19}H_{14}BrNO$): 351.0253, found: 351.0253.

Synthesis of 10-(4-(4,4,5,5-tetramethyl-1,3,2-dioxaborolan-2-yl)phenyl)-10*H*-phenoxazines 1a,b. General procedure.

10-(4-Bromophenyl)-10*H*-phenoxazine (**6a**) (0.54 g, 1.6 mmol) or 10-(4-bromo-3-methylphenyl)-10*H*-phenoxazine (**6b**) (0.57 g, 1.6 mmol), $PdCl_2dppf*CH_2Cl_2$ (0.13 g, 0.16 mmol, 10 mol %), bis(pinacolato)diboron (1.3 equiv., 0.53 g, 2.1 mmol), KOAc (5 equiv., 0.8 g, 8.0 mmol) and dioxane (5 mL) were placed in a screw-cap vial equipped with a magnetic stir bar. The vial was purged with argon and the reaction mixture was stirred vigorously at 110 °C for 24 h under argon atmosphere. After completion of the reaction, water (20 mL) was added and the aqueous solution was extracted with chloroform (4×20 mL). The combined extract was dried with anhydrous Na_2SO_4, filtered and chloroform was removed by distillation under reduced pressure. Residue was purified by column chromatography using chloroform:petroleum ether (1:2) as an eluent to give the corresponding compounds **1a,b**.

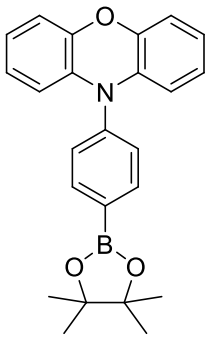

Figure S4. Molecular structure of 10-(4-(4,4,5,5-tetramethyl-1,3,2-dioxaborolan-2-yl)phenyl)-10*H*-phenoxazine **(1a).**

White solid (0.35 g, 56%), mp 149-151 °C. ^{1}H NMR (400 MHz, $CDCl_3$) δ (ppm): 1.45 (12H, s, 4xCH_3), 5.99 (2H, d, *J* = 8 Hz, phenoxazine-1,9-H), 6.61-6.76 (6H, m, phenoxazine-2-4,6-8-H), 7.43 (2H, d, *J* = 8 Hz, Ph-2,6-H), 8.12 (2H, d, *J* = 8 Hz, Ph-3,5-H). ^{11}B NMR (128.4 MHz, $CDCl_3$) δ (ppm): 30.22.
NMR spectra and melting point of compound **1a** match with those described in ref[2].

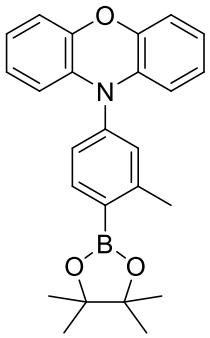

Figure S5. Molecular structure of 10-(3-methyl-4-(4,4,5,5-tetramethyl-1,3,2-dioxaborolan-2-yl)phenyl)-10*H*-phenoxazine **(1b).**

White solid (0.37 g, 58%), mp 156-158 °C. ^{1}H NMR (400 MHz, DMSO-d_6) δ (ppm): 1.42 (12H, s, 4xCH_3), 2.63 (3H, s, CH_3), 5.97 (2H, d, *J* = 8 Hz, phenoxazine-1,9-H), 6.60 – 6.72 (6H, m, phenoxazine-2-4,6-8-H), 7.18-7.19 (2H, m, Ph-2,6-H), 8.01 (1H, d, *J* = 8 Hz, Ph-5- H). ^{13}C NMR (100 MHz, $CDCl_3$) δ (ppm): 22.2, 24.9, 83.8, 113.3, 113.4, 115.3, 121.2, 123.2, 126.9, 131.7, 134.2, 138.5, 141.1, 143.9, 148.2. ^{11}B NMR (128.4 MHz, $CDCl_3$) δ (ppm): 32.14. HRMS-ESI: m/z calcd. for $[M]^+$ ($C_{25}H_{26}BNO_3$): 399.2005, found: 399.2005.

Synthesis of 3-methyl-4-(10*H*-phenoxazin-10-yl)phenylboronic acid (2).

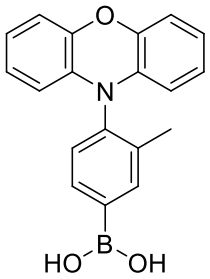

Figure S6. Molecular structure of 3-methyl-4-(10*H*-phenoxazin-10-yl)phenylboronic acid **(2).**

To a solution of 10-(4-bromo-2-methylphenyl)-10*H*-phenoxazine (**6c**) (1.0 g, 2.84 mmol) in 50 mL of anhydrous tetrahydrofuran 2.5 M *n*-butyllithium solution in hexanes (1.5 equiv., 1.7 mL, 4.26 mmol) was added dropwise at −78 °C under argon atmosphere and vigorous stirring. After stirring for 1 h, trimethyl borate (1.8 equiv., 0.58 mL, 5.11 mmol) was added at the same temperature and allowed to warm to room temperature overnight under stirring. Then 1 M hydrochloric acid was added dropwise until an acidic solution was obtained. After stirring for 1 h, the reaction mixture was poured into water and extracted with chloroform (4×40 mL). The combined organic layer was dried over anhydrous Na_2SO_4, filtered and evaporated to dryness. The crude product was then purified by precipitating with petroleum ether to give compound **2** as a yellowish solid (0.61 g, 68%) and used in cross-coupling reaction without additional purification. ^{1}H NMR (400 MHz, DMSO-d_6) δ (ppm): 2.77 (3H, s, CH_3), 5.91 – 5.93 (2H, m, phenoxazine-1,9-H), 6.63 – 6.67 (6H, m, phenoxazine-2-4,6-8-H), 7.15 – 7.20 (2H, m, Ph-5,6-H), 8.20 (1H, d, *J* = 8 Hz, Ph-3-H). HRMS-ESI: m/z calcd. for $[M]^+$ ($C_{19}H_{16}BNO_3$): 317.1221, found: 317.1221.

Synthesis of 4,6-bis(4-(10*H*-phenoxazin-10-yl)phenyl)pyrimidines PXZ-PYR and PXZ-mdPYR.

Compounds **PXZ-PYR** and **PXZ-mdPYR** were synthesized by the Suzuki-Myiaura cross-coupling reaction according to the scheme S2.

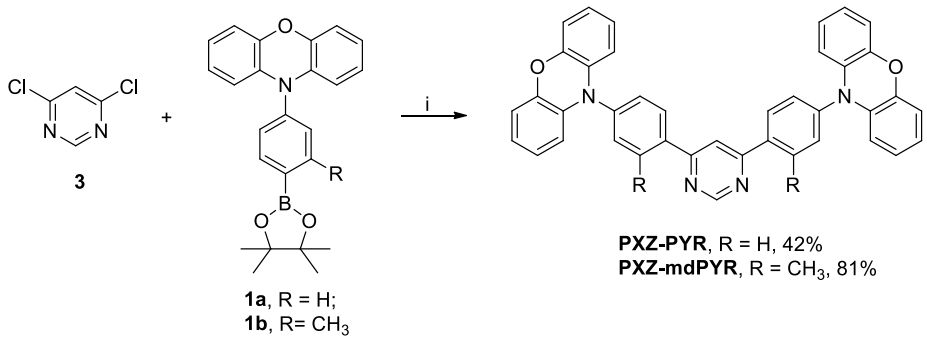

Scheme S2. *Reagents and conditions*: i) corresponding boronic ester (2.2 equiv.), $Pd(PPh_3)_4$ (10 mol%), aq. K_2CO_3 (15 equiv.), glyme, 80 °C, 24 h.

Synthesis of compounds PXZ-PYR and PXZ-mdPYR. General procedure.

4,6-Dichloropyrimidine (**3**) (50 mg, 0.336 mmol), $Pd(PPh_3)_4$ (39 mg, 0.034 mmol, 10 mol %), corresponding boronic ester **1a** or **1b** (2.2 equiv., 0.726 mmol) and 2 ml of aqueous K_2CO_3 (15 equiv., 0.7 g, 4.95 mmol) and glyme (3 mL) were placed in a screw-cap vial equipped with a magnetic stir bar. The reaction mixture was stirred vigorously at 80 °C for 24 h under argon atmosphere. After completion of the reaction, water (20 mL) was added and the aqueous solution was extracted with chloroform (4×20 mL). The combined extract was dried with anhydrous Na_2SO_4, filtered and chloroform was removed by distillation under reduced pressure. Residue was purified by column chromatography using chloroform:petroleum ether (1:2) as an eluent to give the corresponding **PXZ-PYR** and **PXZ-mdPYR**.

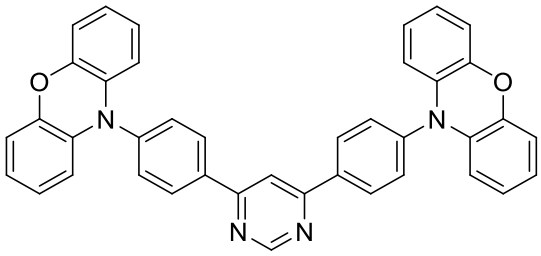

Figure S7. Molecular structure of 4,6-bis(4-(10*H*-phenoxazin-10-yl)phenyl)pyrimidine **(PXZ-PYR).**

Starting with 4,6-dichloropyrimidine (**3**) and 10-(4-(4,4,5,5-tetramethyl-1,3,2-dioxaborolan-2-yl)phenyl)-10*H*-phenoxazine (**1a**), compound **PXZ-PYR** was obtained as a yellow solid (84 mg, 42%), mp 163-165 °C. ^{1}H NMR (400 MHz, $CDCl_3$) δ (ppm): 6.05 (4H, d, *J* = 8 Hz, 2x-phenoxazine-1,9-H), 6.65-6.77 (12H, m, 2x-phenoxazine-2-4,6-8-H), 7.59 (4H, d, *J* = 8 Hz, 2xPh-3,5-H), 8.26 (1H, s, pyrimidine-5-H), 8.44 (4H, d, *J* = 8 Hz, 2xPh-2,6-H), 9.44 (1H, s, pyrimidines-2-H).
NMR spectra of compound **PXZ-PYR** match with those described in ref[3].

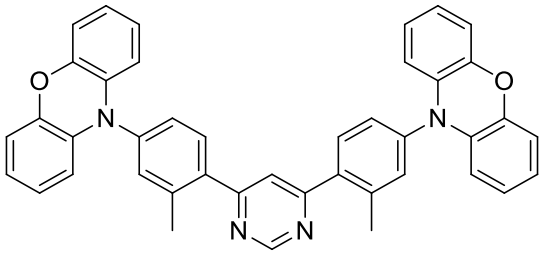

Figure S8. Molecular structure of 4,6-bis(2-methyl-4-(10*H*-phenoxazin-10-yl)phenyl)pyrimidine **(PXZ-mdPYR).**

Starting with 4,6-dichloropyrimidine (**3**) and 10-(3-Methyl-4-(4,4,5,5-tetramethyl-1,3,2-dioxaborolan-2-yl)phenyl)-10H-phenoxazine (**1b**), compound **PXZ-mdPYR** was obtained as a yellow solid (170 mg, 81%), mp 278 °C. ^{1}H NMR (400 MHz, $CDCl_3$) δ (ppm): 2.60 (6H, s, 2xCH_3), 6.05 (4H, d, *J* = 8 Hz, 2x-phenoxazine-1,9-H), 6.65-6.75 (12H, m, 2x-phenoxazine-2-4,6-8-H), 7.38 (4H, d, *J* = 8 Hz, 2xPh-3,5-H), 7.76-7.80 (3H, m, pyrimidine-5-H, 2x-Ph-6-H), 9.48 (1H, s, pyrimidine-2-H). ^{13}C NMR (100 MHz, $CDCl_3$) δ (ppm): 20.7, 113.4, 115.6, 121.6, 122.9, 123.3, 128.7, 132.5, 133.4, 134.1, 137.9, 139.6, 140.3, 143.9, 158.5, 166.7. HRMS-ESI: m/z calcd. for $[M+H]^+$ ($C_{42}H_{31}N_4O_2$): 623.2442, found: 623.2443.

Synthesis of 4,6-bis(3-methyl-4-(10H-phenoxazin-10-yl)phenyl)pyrimidine (PXZ-muPYR)

Compound **PXZ-muPYR** were synthesized by the Suzuki-Myiaura cross-coupling reaction according to the scheme S3.

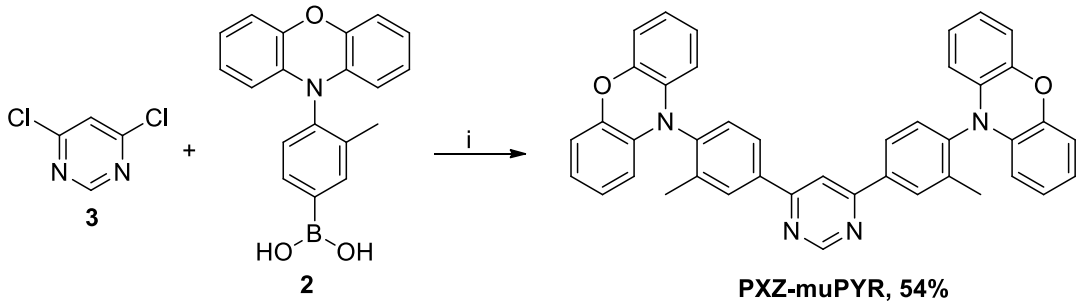

Scheme S3. *Reagents and conditions*: i) boronic acid (2.5 equiv.), $Pd(OAc)_2$ (10 mol%), PPh_3 (20 mol%), aq. Na_2CO_3 (6.2 equiv.), glyme, 90 ºC, 24 h.

Synthesis of PXZ-muPYR. 4,6-Dichloropyrimidine (**3**) (50 mg, 0.336 mmol), $Pd(OAc)_2$ (7.5 mg, 0.034 mmol, 10 mol %), PPh_3 (17.6 mg, 0.067 mmol, 20 mol %), 3-methyl-4-(10*H*-phenoxazin-10-yl)phenylboronic acid (**2**) (0.829 mmol, 2.5 equiv.), 2 mL of aqueous Na_2CO_3 (6.2 equiv., 221 mg, 2.08 mmol) and glyme (3 mL) were placed in a screw-cap vial equipped with a magnetic stir bar. The reaction mixture was stirred vigorously at 90 °C for 24 h under argon atmosphere. After completion of the reaction, water (20 mL) was added and the aqueous solution was extracted with chloroform (4×20 mL). The combined extract was dried with anhydrous Na_2SO_4, filtered and chloroform was removed by distillation under reduced pressure. Residue was purified by column chromatography using chloroform:petroleum ether (1:2) as eluent to give **PXZ-muPYR** as a yellow solid (0.11 g, 54%), mp 283

°C. ^{1}H NMR (400 MHz, $CDCl_3$) δ (ppm): 2.40 (6H, s, 2xCH_3), 5.88 (4H, d, *J* = 8 Hz, 2x-phenoxazine-1,9-H), 6.61-6.75 (12H, m, 2x-phenoxazine-2-4,6-8-H), 7.51 (2H, d, *J* = 8 Hz, 2x-Ph-5-H), 8.20-8.24 (3H, m, pyrimidine-5-H, 2xPh-2,6-H), 9.42 (1H, s, pyrimidine-2-H). ^{13}C NMR (100 MHz, $CDCl_3$) δ (ppm): 17.9, 112.6, 113.3, 115.6, 121.5, 123.5, 127.5, 131.2, 132.0, 133.0, 137.4, 139.7, 140.2, 143.9, 159.4, 164.2. HRMS-ESI: m/z calcd. for $[M+H]^+$ ($C_{42}H_{31}N_4O_2$): 623.2442, found: 623.2439.

Synthesis of 4,6-bis(2,5-dimethyl-4-(10*H*-phenoxazin-10-yl)phenyl)pyrimidine (PXZ-2mPYR).
Compound **PXZ-2mPYR** was synthesized by cross-coupling of 4,6-bis(4-bromo-2,5-dimethylphenyl)pyrimidine (**4**)[4] with phenoxazine under the palladium-catalyzed Buchwald-Hartwig reaction conditions (Scheme S4).

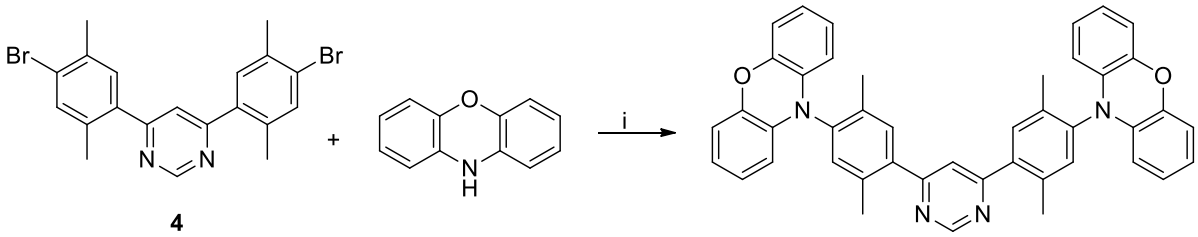

Scheme S4*. Reagents and conditions*: i) phenoxazine (2.2 equiv.), Pd_2dba_3 (5 mol%), P(*t*-Bu)$_3$*HBF_4 (10 mol%), NaO*t*-Bu (3 equiv.), toluene, Ar, 110 °C, 24 h.

Synthesis of PXZ-2mPYR. 4,6-Bis(4-bromo-2,5-dimethylphenyl)pyrimidine (**4**) (50 mg, 0.11 mmol), Pd_2dba_3 (5.1 mg, 0.0055 mmol, 5 mol%), P(*t*-Bu)$_3$*HBF_4 (3.3 mg, 0.011 mmol, 10 mol%), phenoxazine (2.2 equiv., 45 mg, 0.24 mmol), NaO*t*-Bu (3 equiv., 32 mg, 0.33 mmol) and toluene (2 mL) were placed in a screw-cap vial equipped with a magnetic stir bar. The reaction mixture was stirred vigorously at 100 °C for 24 h under argon atmosphere. After completion of the reaction, water (20 mL) was added and the aqueous solution was extracted with chloroform (4×20 mL). The combined extract was dried with anhydrous Na_2SO_4, filtered, and chloroform was removed by distillation under reduced pressure. Residue was purified by column chromatography using chloroform:petroleum ether (1:2) as eluent to give **PXZ-2mPYR** as a yellow solid (69 mg, 95%), mp 223-225 °C. ^{1}H NMR (400 MHz, $CDCl_3$) δ (ppm): 2.31 (6H, s, 2xCH_3), 2.55 (6H, s, 2xCH_3), 5.92 (4H, d, *J* = 8 Hz, 2x-phenoxazine-1,9-H), 6.63-6.75 (12H, m, 2x-phenoxazine-2-4,6-8-H), 7.32 (2H, s, 2xPh-3-H), 7.67 (2H, s, 2xPh-6-H), 7.76 (1H, s, pyrimidine-5-H), 9.48 (1H, s, pyrimidine-2-H). ^{13}C NMR (100 MHz, $CDCl_3$) δ (ppm): 17.2, 20.1, 112.7, 115.6, 121.0, 121.4, 123.5, 133.2, 133.55, 133.59, 136.7, 136.9, 138.2, 138.3, 143.9, 158.6, 166.6. HRMS-ESI: m/z calcd. for $[M+H]^+$ ($C_{44}H_{35}N_4O_2$): 651.2755, found: 651.2763.

^{1}H and ^{13}C NMR spectra of the synthesized new compounds

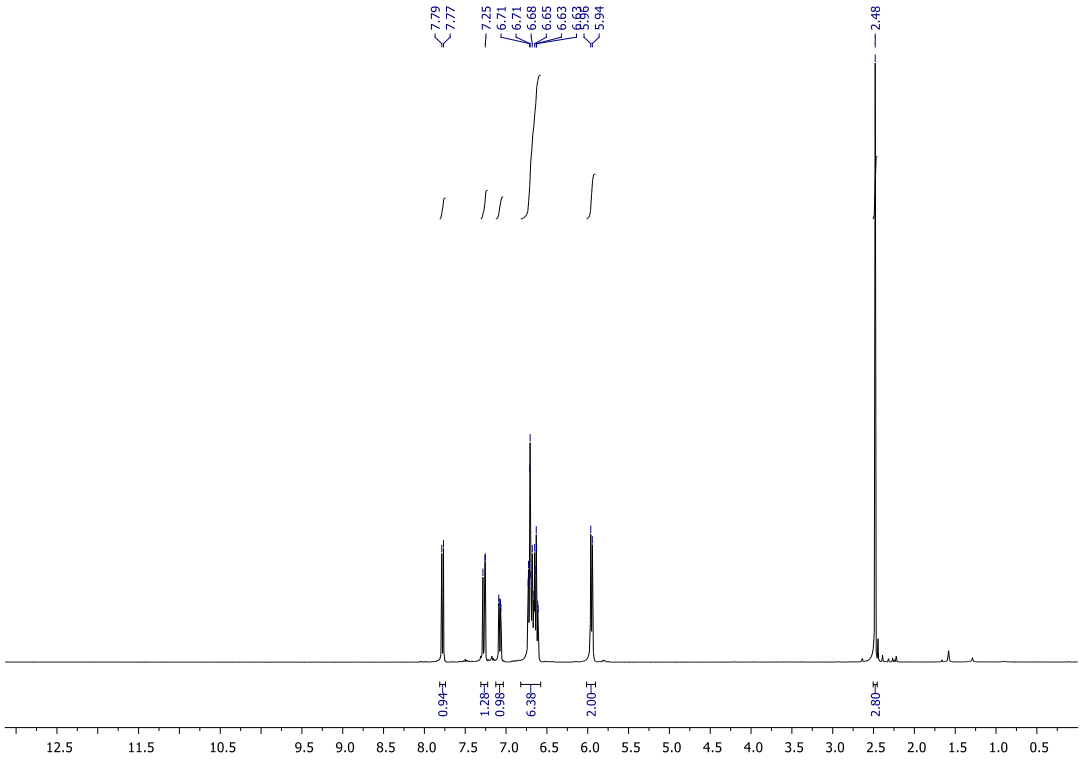

Figure S9. ^{1}H NMR spectrum of 10-(4-Bromo-3-methylphenyl)-10*H*-phenoxazine **(6b).**

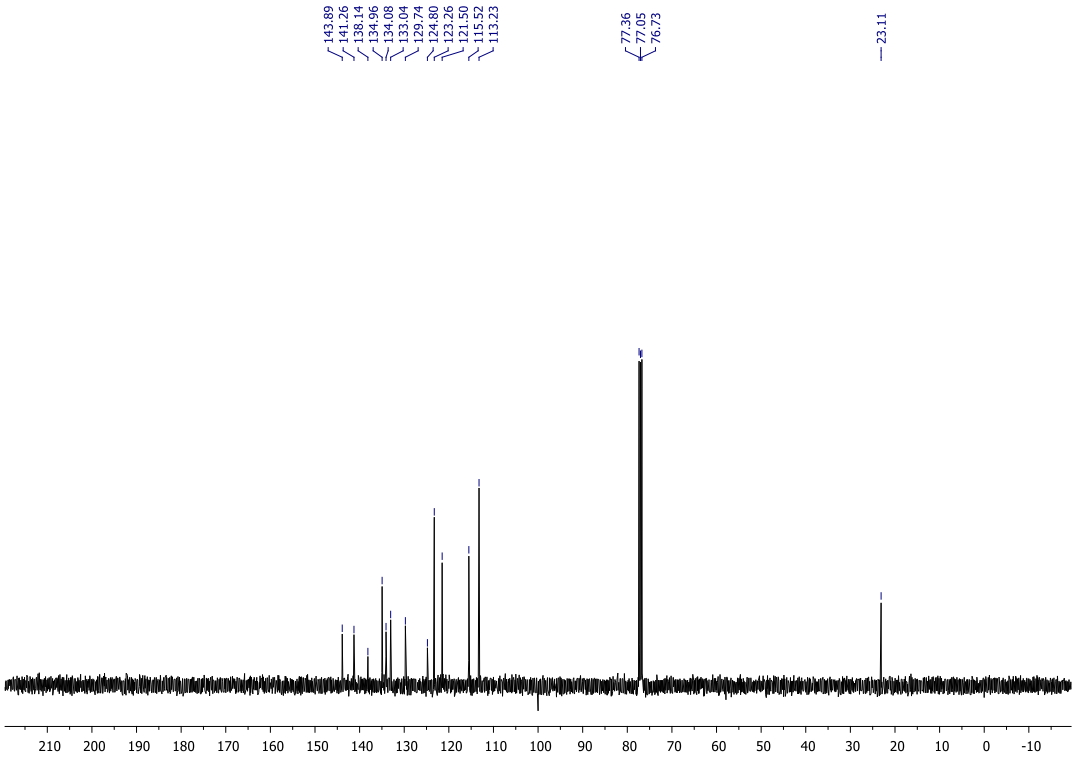

Figure S10. ^{13}C NMR spectrum of 10-(4-Bromo-3-methylphenyl)-10*H*-phenoxazine **(6b)**

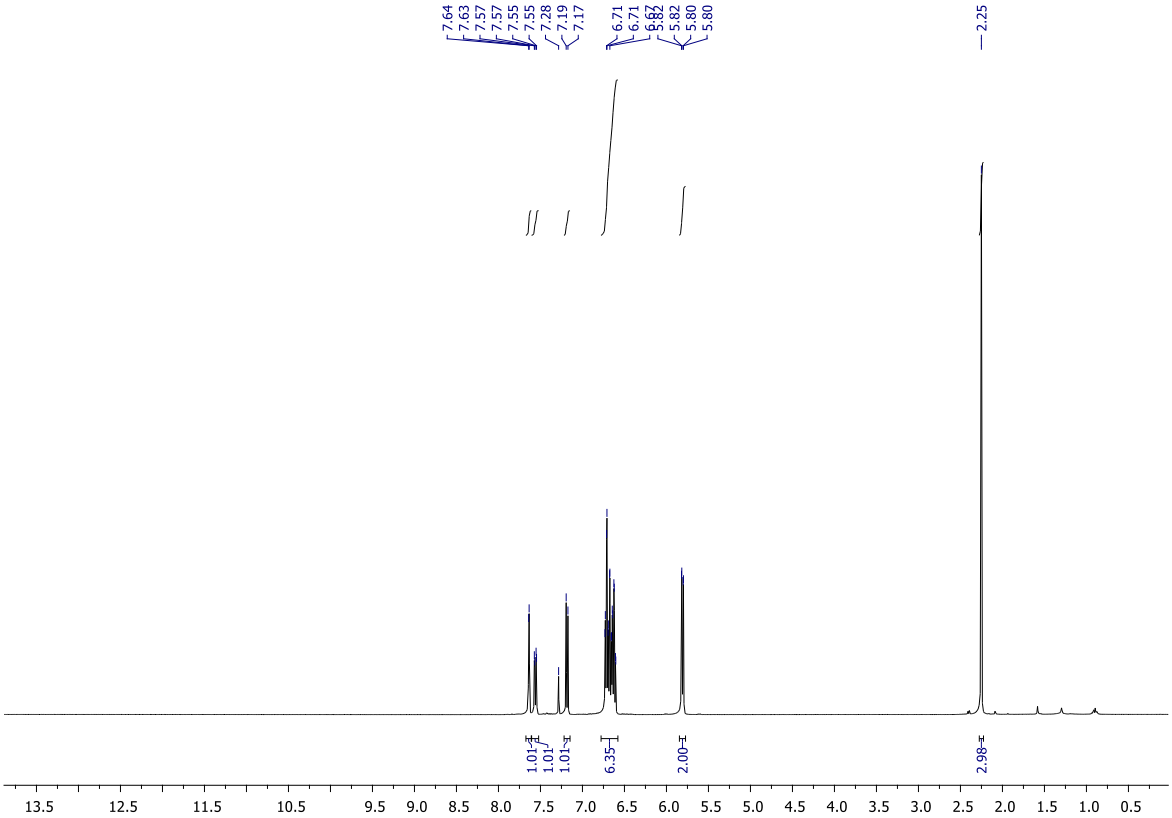

Figure S11. ^{1}H NMR spectrum of 10-(4-bromo-2-methylphenyl)-10*H*-phenoxazine **(6c).**

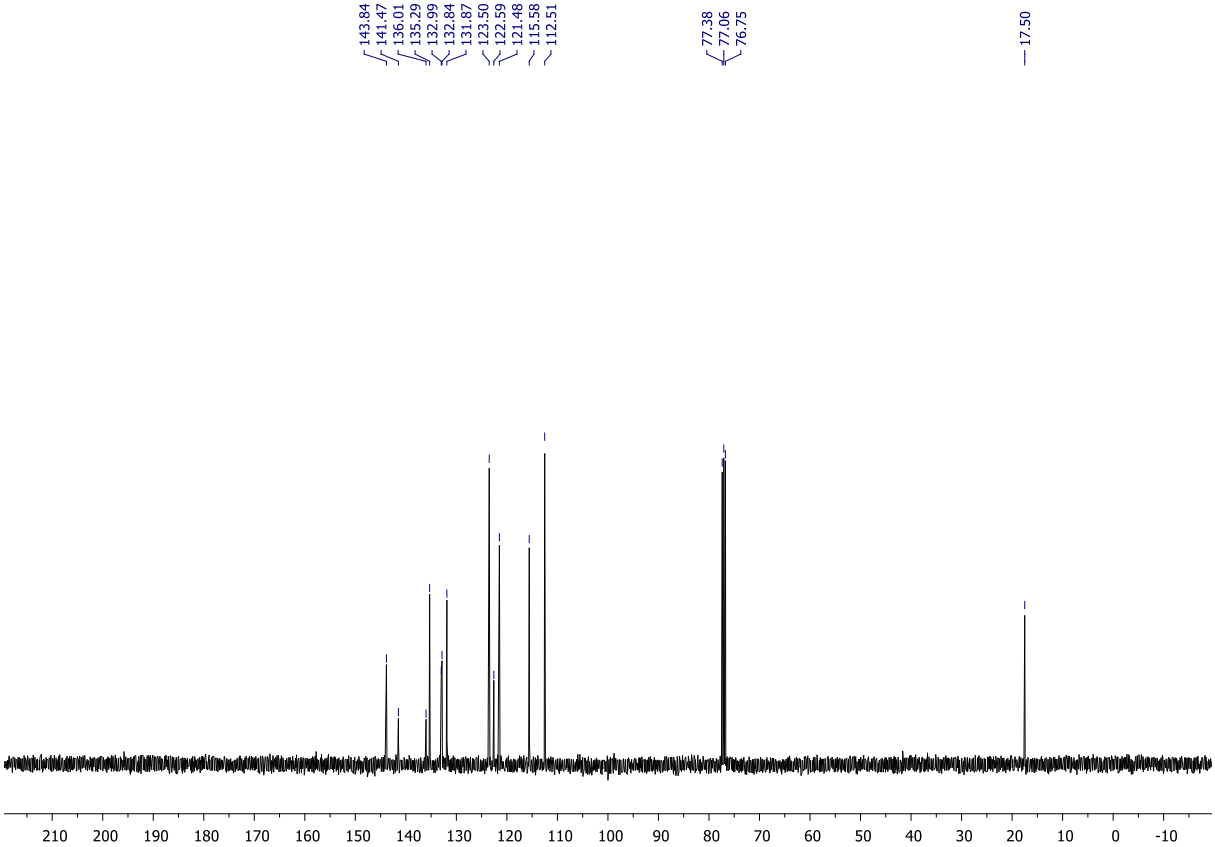

Figure S12. ^{13}C NMR spectrum of 10-(4-bromo-2-methylphenyl)-10*H*-phenoxazine **(6c).**

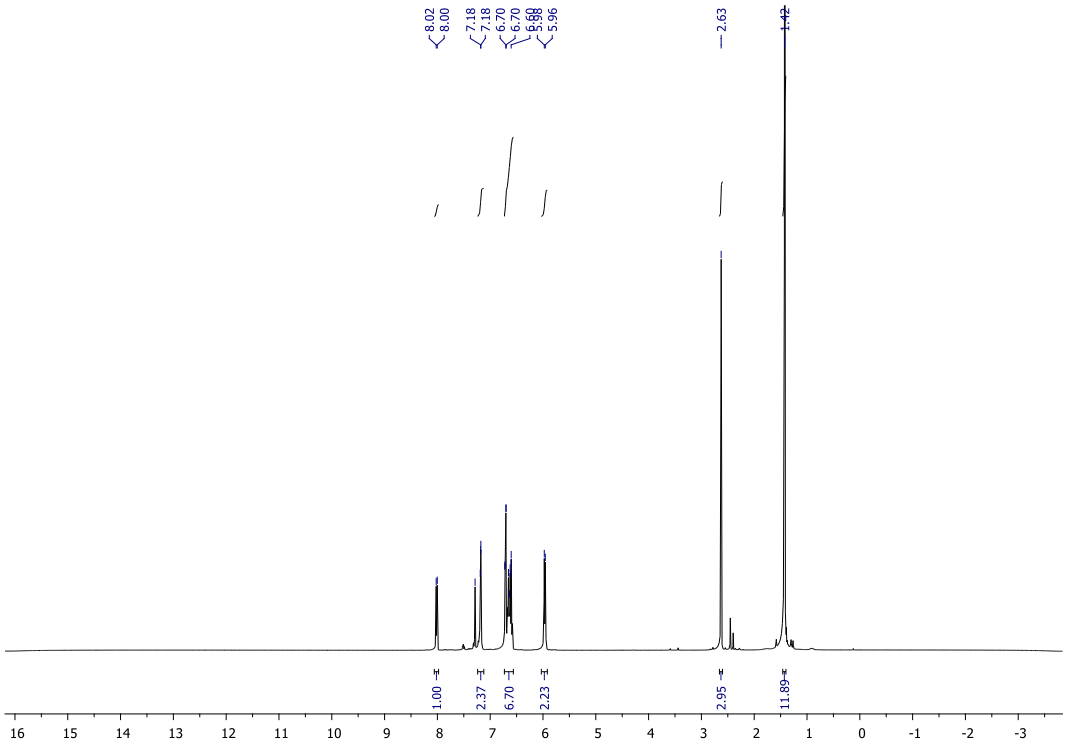

Figure S13. ^{1}H NMR spectrum of 10-(3-methyl-4-(4,4,5,5-tetramethyl-1,3,2-dioxaborolan-2-yl)phenyl)-10*H*-phenoxazine **(1b).**

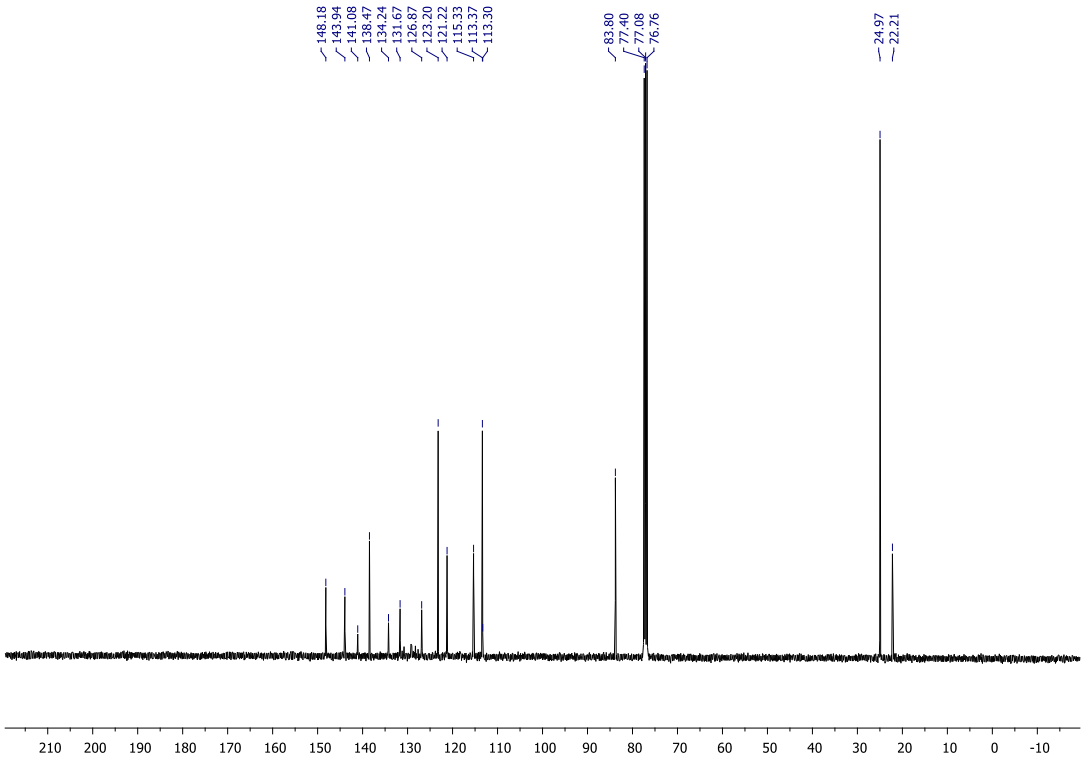

Figure S14. ^{13}C NMR spectrum of 10-(3-methyl-4-(4,4,5,5-tetramethyl-1,3,2-dioxaborolan-2-yl)phenyl)-10*H*-phenoxazine **(1b).**

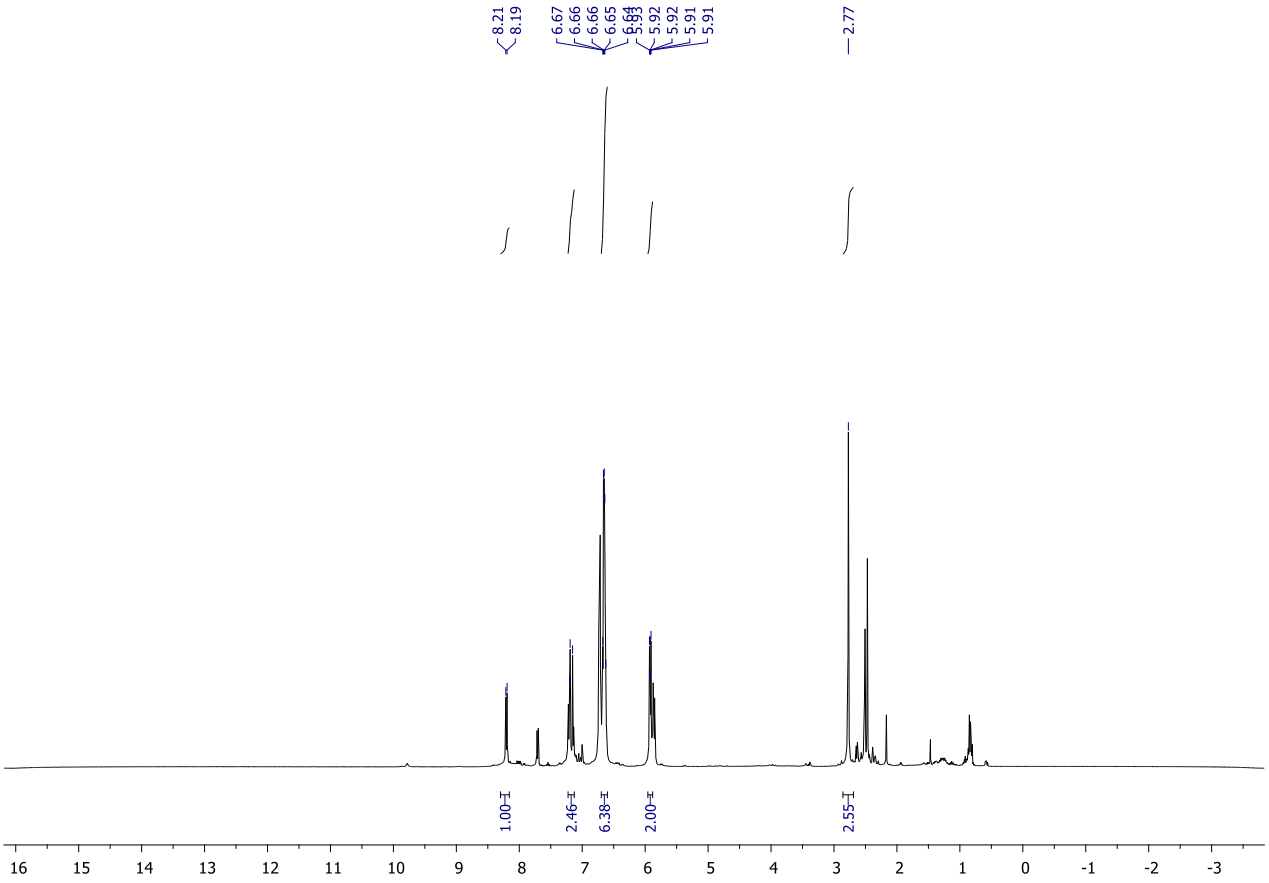

Figure S15. ^{1}H NMR spectrum of 3-methyl-4-(10*H*-phenoxazin-10-yl)phenylboronic acid **(2).**

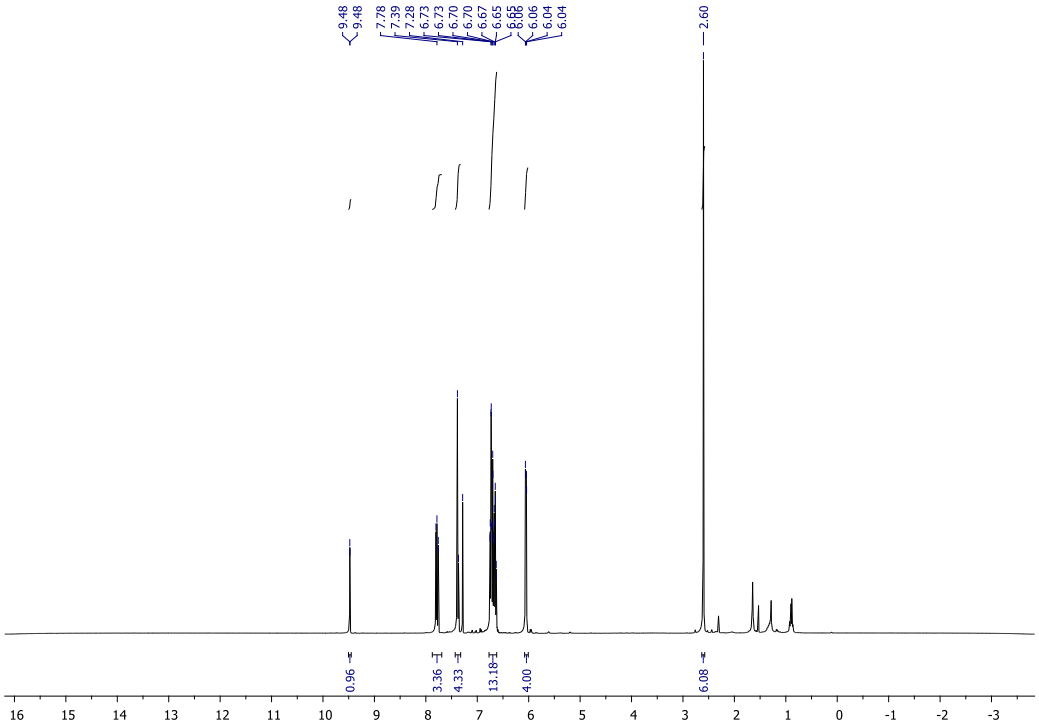

Figure S16. ^{1}H NMR spectrum of 4,6-bis(2-methyl-4-(10*H*-phenoxazin-10-yl)phenyl)pyrimidine **(PXZ-mdPYR).**

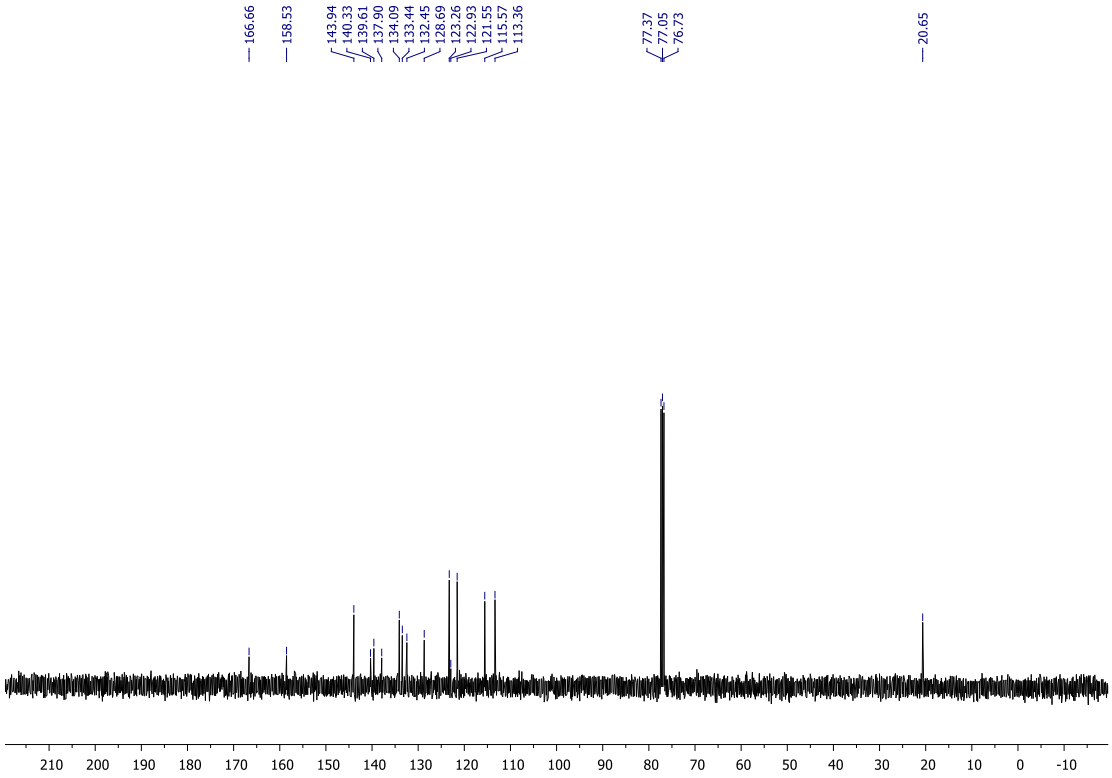

Figure S17. ^{13}C NMR spectrum of 4,6-bis(2-methyl-4-(10*H*-phenoxazin-10-yl)phenyl)pyrimidine **(PXZ-mdPYR).**

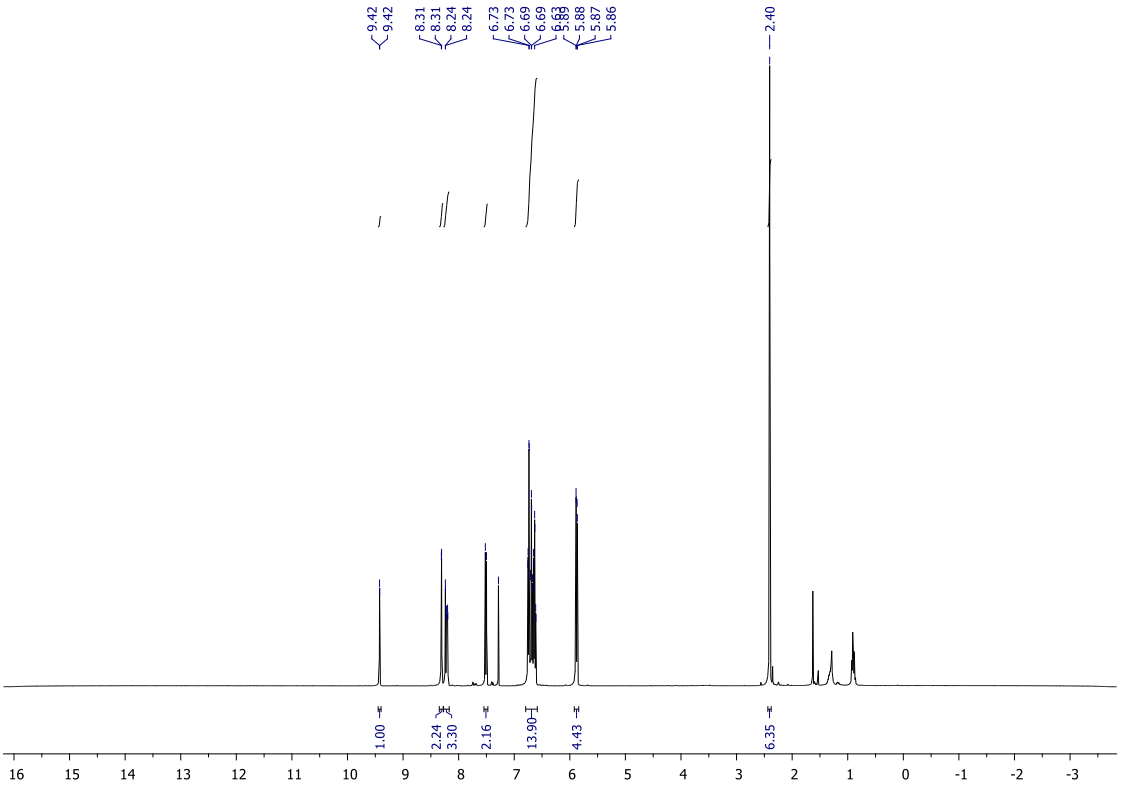

Figure S18. ^{1}H NMR spectrum of 4,6-bis(3-methyl-4-(10*H*-phenoxazin-10-yl)phenyl)pyrimidines **(PXZ-muPYR).**

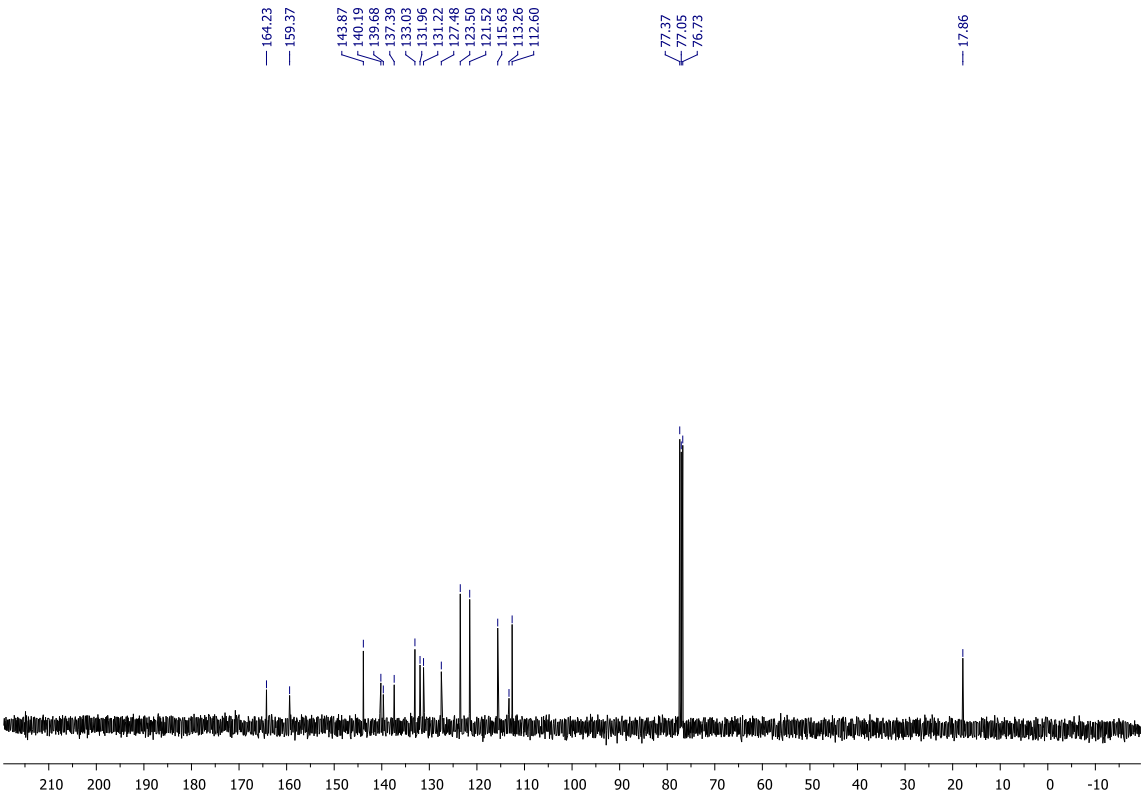

Figure S19. ^{13}C NMR spectrum of 4,6-bis(3-methyl-4-(10*H*-phenoxazin-10-yl)phenyl)pyrimidines **(PXZ-muPYR).**

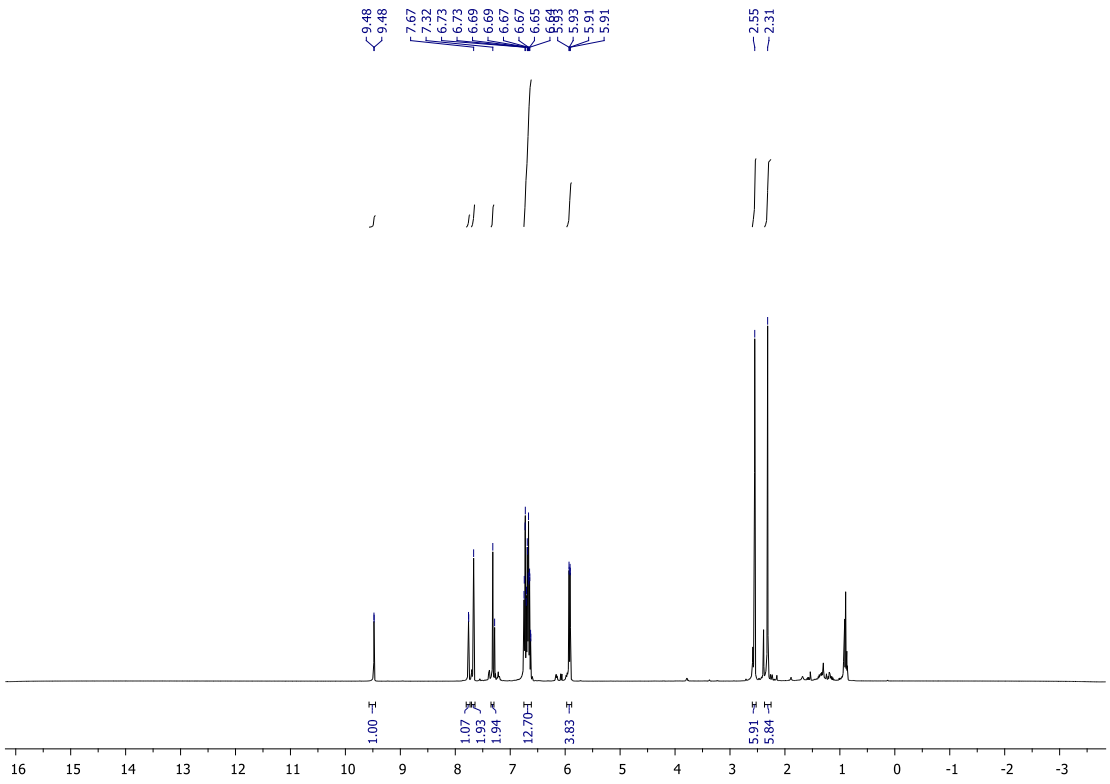

Figure S20. [1]H NMR spectrum of 4,6-bis(2,5-dimethyl-4-(10*H*-phenoxazin-10-yl)phenyl)pyrimidine **(PXZ-2mPYR)**

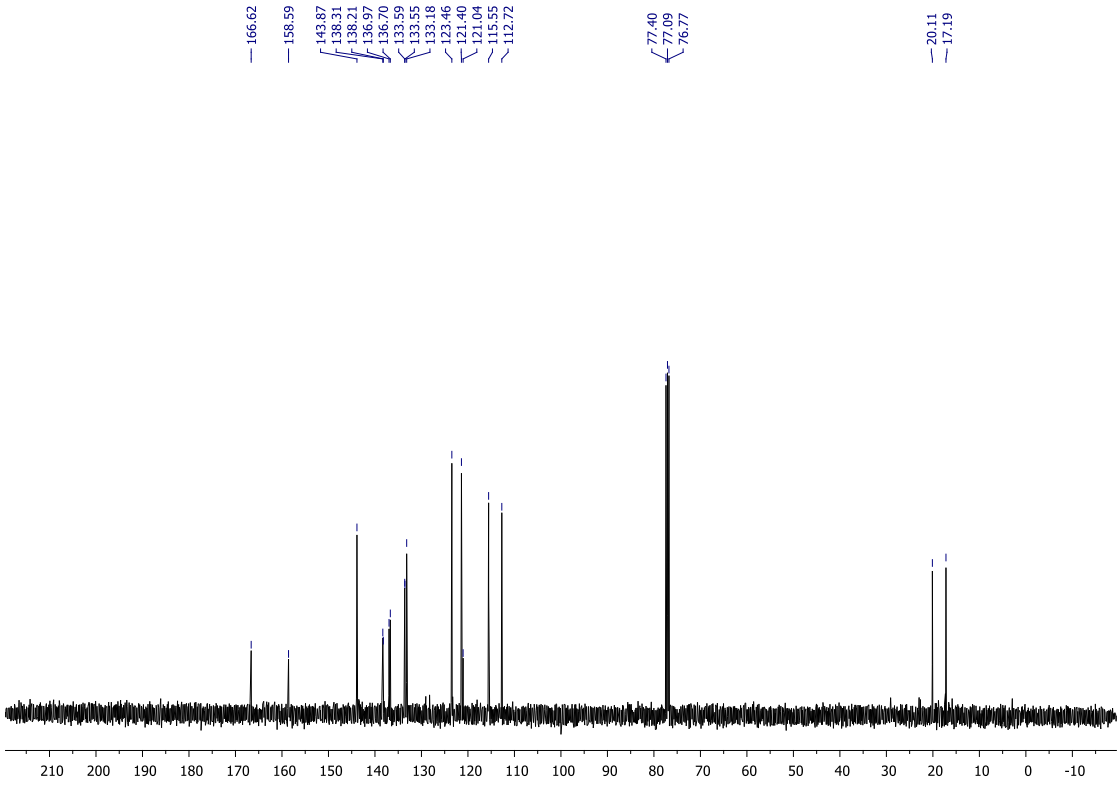

Figure S21. [1]H NMR spectrum of 4,6-bis(2,5-dimethyl-4-(10*H*-phenoxazin-10-yl)phenyl)pyrimidine **(PXZ-2mPYR)**

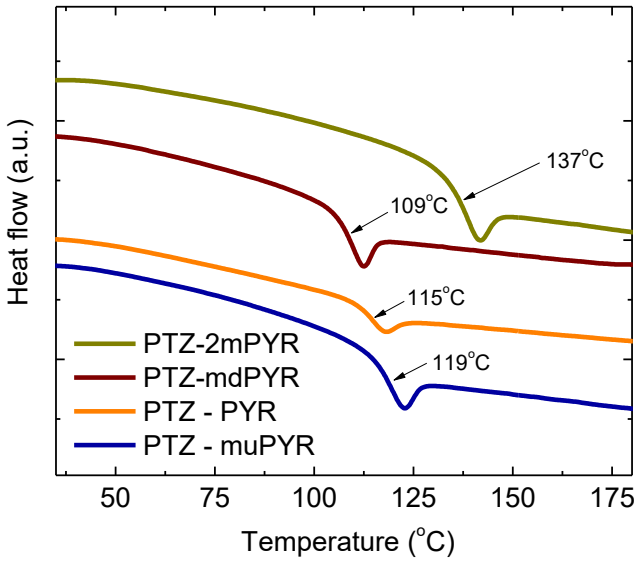

Figure S21 Differential scanning calorimetry thermograms of phenoxazine-pyrimidine TADF compounds at the second heating scan.

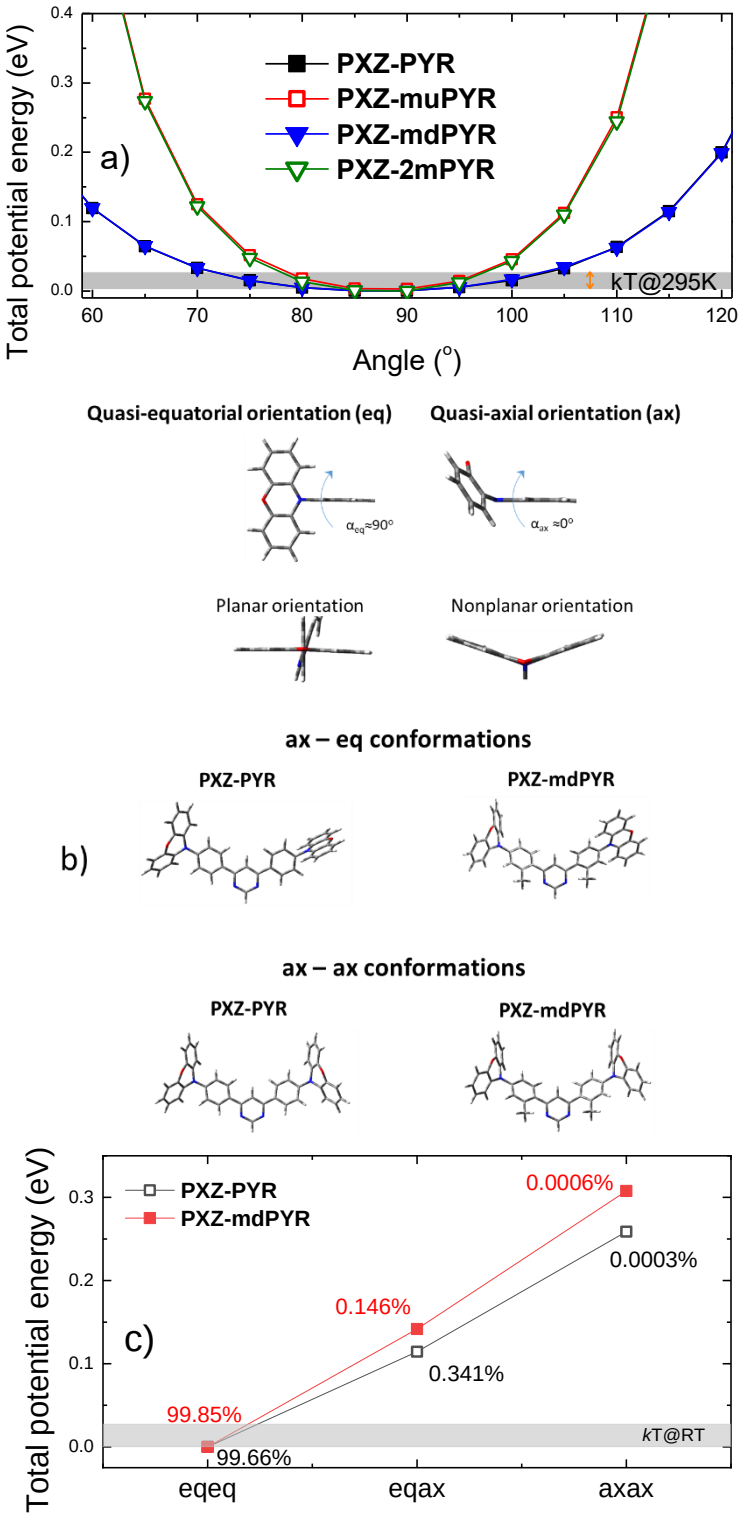

Figure S22 a) Potential energy scans of TADF compounds **PXZ-PYR**, **PXZ-muPYR**, **PXZ-mdPYR** and **PXZ-2mPYR.** Ground state-optimized molecular structure was taken and dihedral angle between the phenyl and phenoxiazine units was varied. No further optimization of molecular structure was performed at the later steps. Energies were normalized to 0. b) Geometry of PXZ unit in quasi-axial (ax) and quasi-equitorial (eq) orientations and DFT optimized ground-state molecular geometries of TADF compounds **PXZ-PYR** and **PXZ-mdPYR** in ax-ax and ax-eq conformations. c) Total potential energies of compounds **PXZ-PYR** and **PXZ-mdPYR** of ground-state optimized eq-eq, eq-ax and ax-ax confomations. Fractional contribution of every conformation is denoted. The shaded area represents the thermal energy at room temperature.

Potential energy scans (PES) were performed for all phenoxazine-pyrimidine compounds to reveal the potential barriers for the twisting of PXZ unit (see Fig.S2 a). Compounds **PXZ-mdPYR** and **PXZ-2mPYR** with the *ortho*-methyl substituents showed very large potential barriers for the twisting of PXZ unit, while for **PXZ-PYR** and **PXZ-muPYR** those barriers were lower, though still much larger than the thermal energy at room temperature. However, since the ground-state optimized molecular geometries with equatorial PXZ orientation were taken for the PES calculation with no further optimization of molecular geometry, somewhat overestimation of potential barriers could be obtained[5]. To estimate the ability for PXZ to form different conformers, the ground-state geometries of **PXZ-PYR** and **PXZ-muPYR** with the lowest potential barriers were optimized in quasi-equatorial (eqeq), quasi-axial (axax) and at the quasi-equatorial - quasi-axial (eqax) orientations and total potential energies were estimated (see Fig. S2 b and c). Typically, PXZ unit in ax orientation was found in the nonplanar orientation[6–8] with remarkably larger potential energies of the corresponding conformers (ax-ax and eq-ax) as compared to eq-eq conformers (of about 114 and 142 meV for ax-eq and 259 and 308 meV for ax-ax for **PXZ-PYR** and **PXZ-muPYR**, respectively). The estimated relative ratios of all PXZ conformations (according to the Boltzman distribution[9]) showed, that eq-eq orientation clearly dominated with 99.66 and 99.85% share for **PXZ-PYR** and **PXZ-muPYR,** respectively. Clearly, only the molecular conformers with quasi-equatorial orientation of the phenoxazine unit can be observed in all the studied compounds.

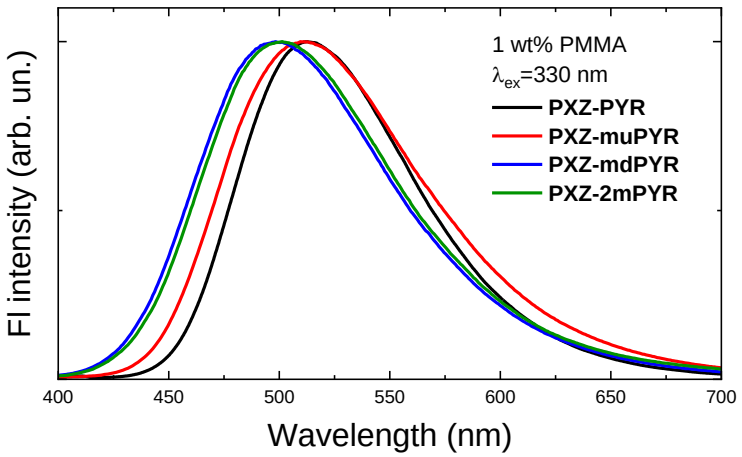

Figure S23 Fluorecence spectra of 1wt% PMMA films of compounds **PXZ-PYR**, **PXZ-muPYR**, **PXZ-mdPYR** and **PXZ-2mPYR**. Emission peaked at 513, 511, 499 and 498 nm for **PXZ-PYR**, **PXZ-muPYR**, **PXZ-mdPYR** and **PXZ-2mPYR**, respectively.

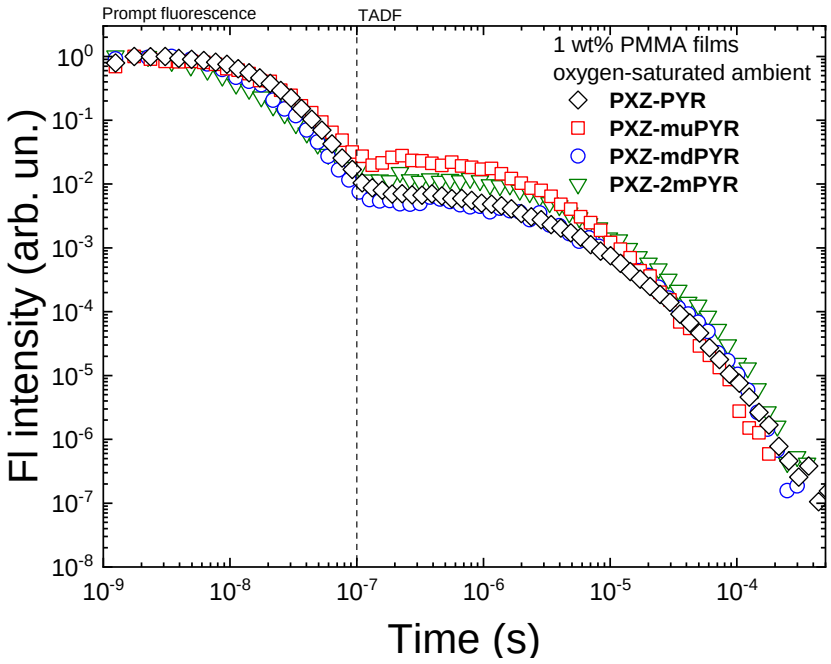

	Φ_F +O_2[a]	PF share[b]	Φ_{PF} +O_2[c]
PXZ-PYR	0.67	0.39	0.26
PXZ-muPYR	0.68	0.23	0.16
PXZ-mdPYR	0.60	0.32	0.19
PXZ-2mPYR	0.41	0.32	0.13

Figure S24 Normalized fluorescence decay transients of 1wt% PMMA films of compounds **PXZ-PYR**, **PXZ-muPYR**, **PXZ-mdPYR** and **PXZ-2mPYR** in oxygen-saturated conditions. The table shows fluorescence quantum yield of phenoxazine-pyrimidine compounds embededd in PMMA films in oxygen-saturated conditions ([a]), prompt fluorescence share in the fluorescence transient of polymer films ([b]) and prompt fluorescence quantum yield of polymer films in oxygen-saturated conditions ([c]). Φ_{PF} +O_2 was estimated according the relation Φ_{PF} +O_2 = Φ_F +O_2 × PF share[10].

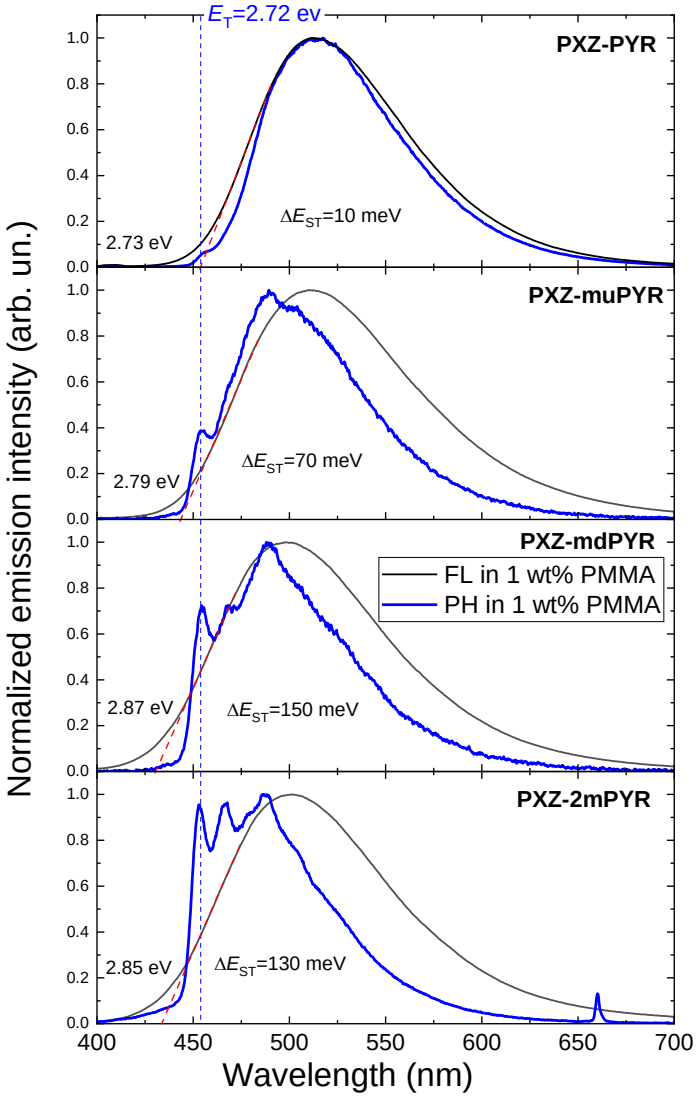

Figure S25 Normalized room temperature time-integrated fluorescence (black lines) and 10 K phosphorescence spectra (blue lines, obtained after 100 μs delay and 890 μs integration time) of 1 wt% PMMA films of compounds **PXZ-PYR**, **PXZ-muPYR**, **PXZ-mdPYR** and **PXZ-2mPYR**. Red dashed lines represent the spectral on-sets of fluorescence spectra.

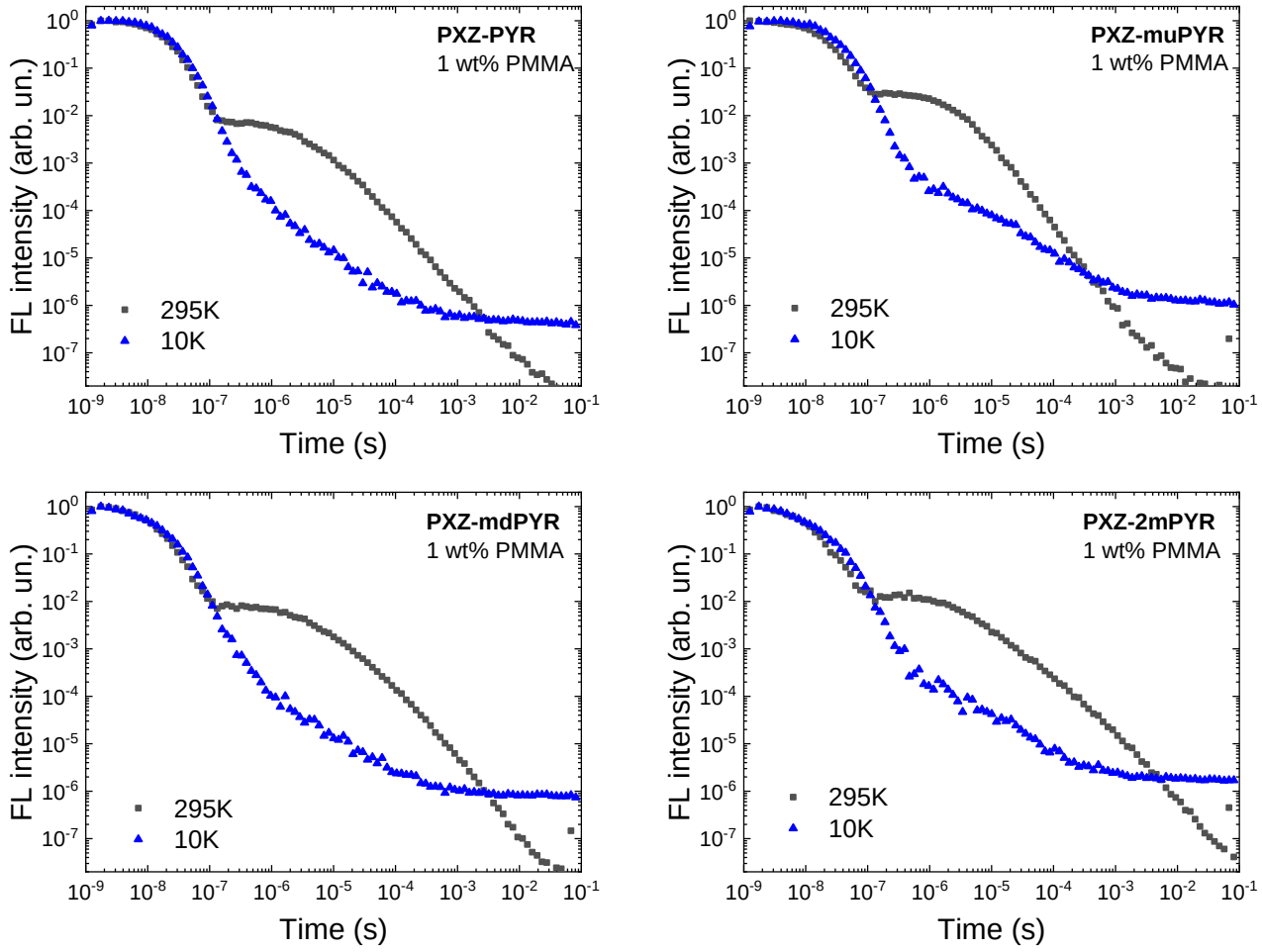

Figure S26 Room temperature (black squares) and 10 K (blue triangles) emission decay transients of 1 wt% PMMA films of compounds **PXZ-PYR**, **PXZ-muPYR**, **PXZ-mdPYR** and **PXZ-2mPYR**.

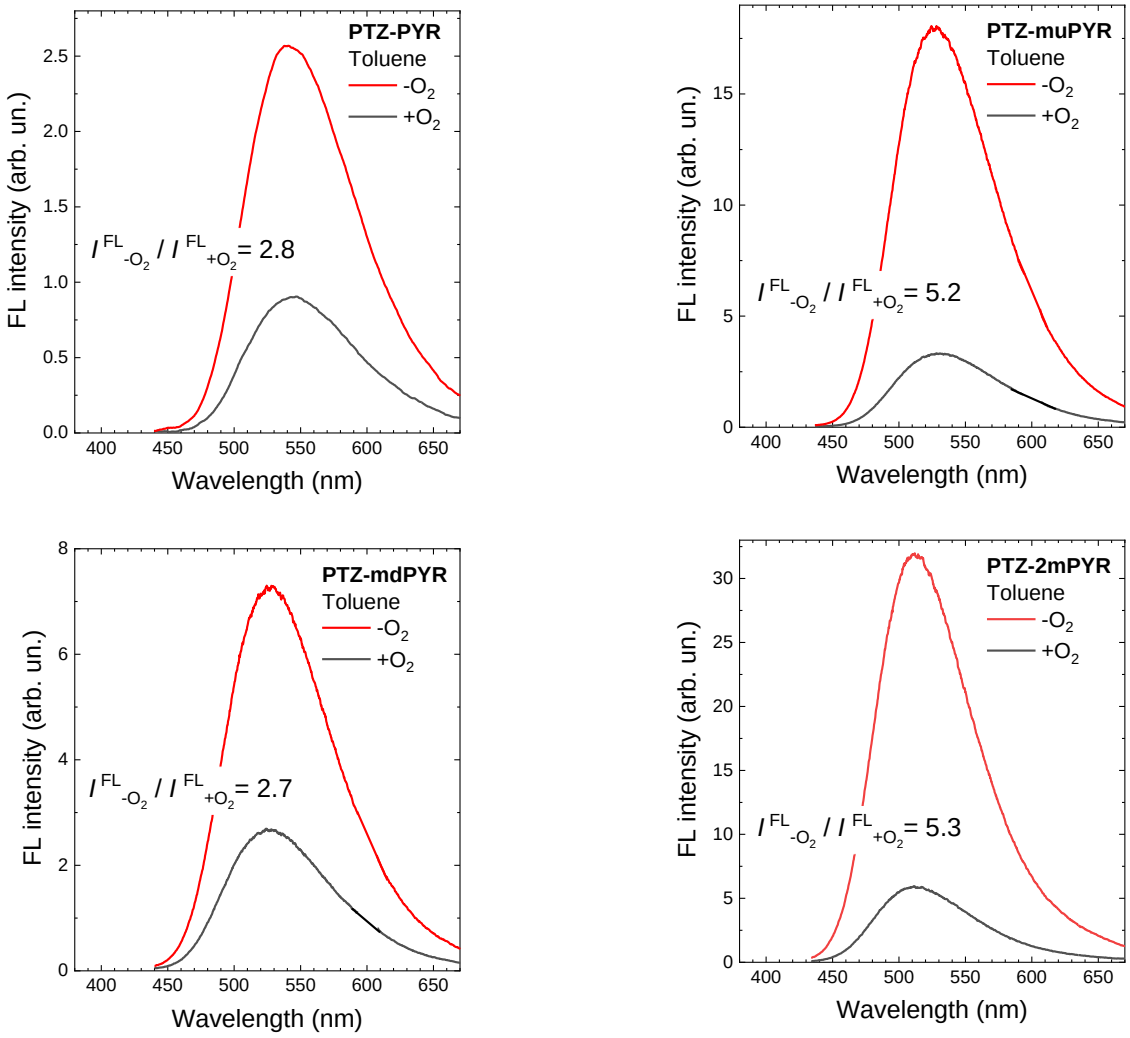

Figure S27 Fluorescence spectra of compounds **PXZ-PYR**, **PXZ-muPYR**, **PXZ-mdPYR** and **PXZ-2mPYR** in oxygen-saturated ($+O_2$) and –deficient ($-O_2$) toluene.

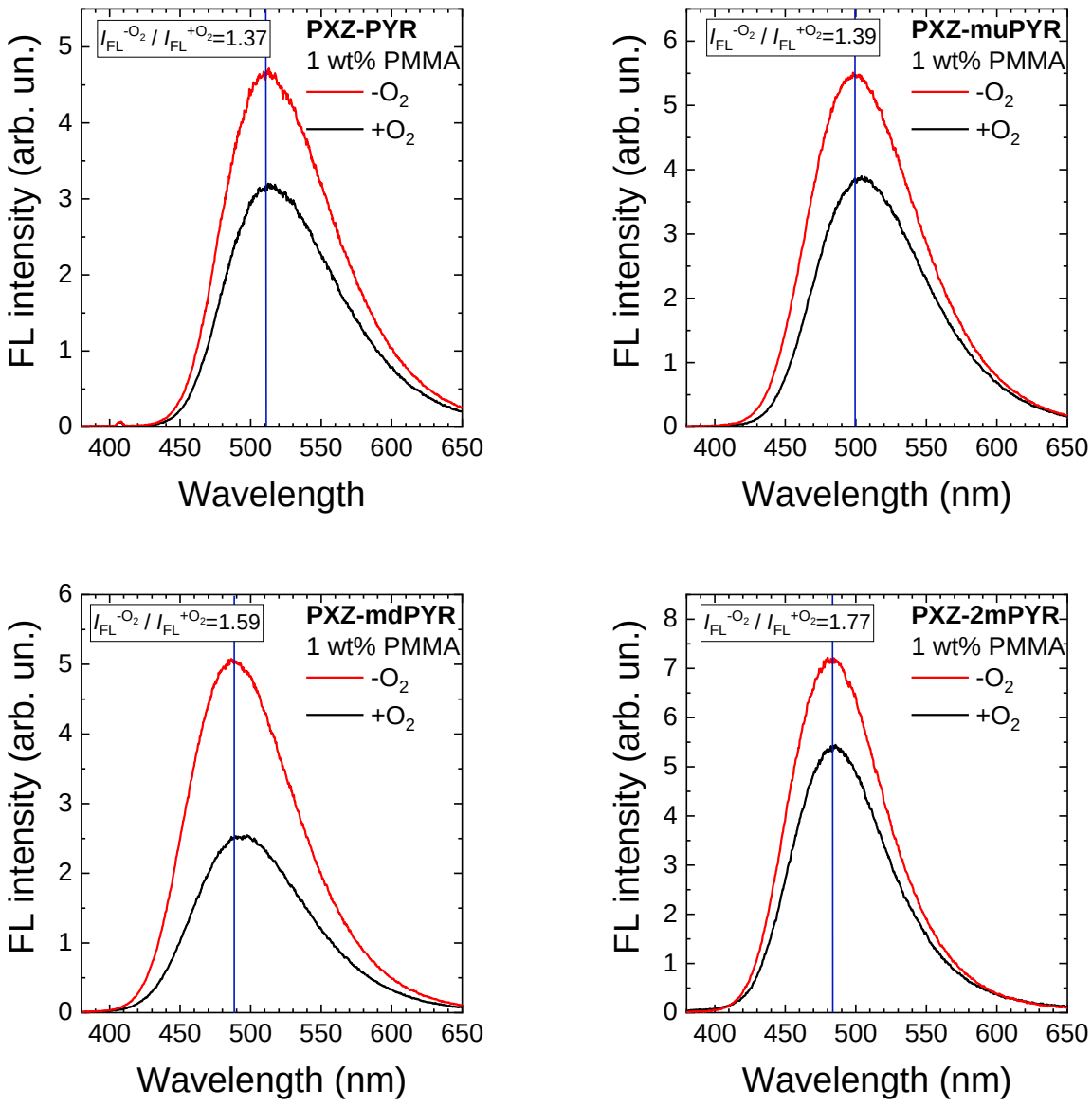

Figure S28 Fluorescence spectra of 1 wt% PMMA films of compounds **PXZ-PYR**, **PXZ-muPYR**, **PXZ-mdPYR** and **PXZ-2mPYR** in oxygen-saturated ($+O_2$) and –deficient ($-O_2$) ambient.

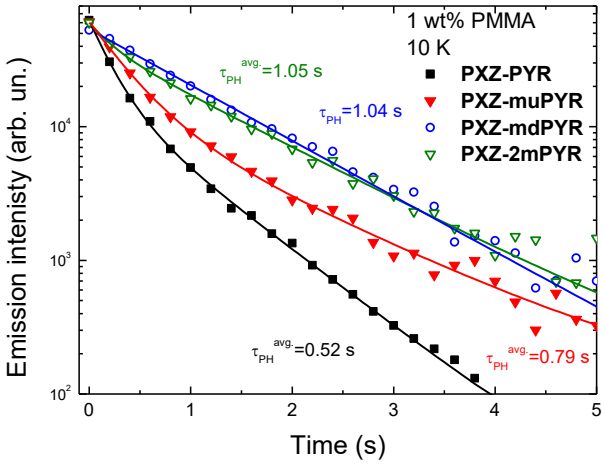

Figure S29 Normalized phosphorescence decay transients of 1 wt% PMMA films of compounds **PXZ-PYR**, **PXZ-muPYR**, **PXZ-mdPYR** and **PXZ-2mPYR** at 10 K temperature. Solid lines are biexponential fits.

Table S1. k_{rISC} values, obtained according to Dias *et.al.*[11] and Wada *et.al.*[12] (when k_{rISC} is comparable to k_r and k_{ISC})).

	k_{rISC} estimated according to Dias *et.al.*[11]				k_{rISC} estimated according to Wada *et.al.*[12]	
	Φ_{ISC}	k_{TADF} ($\times 10^5$ s^{-1})	Φ_{DF}/Φ_{PF}	$\boldsymbol{k_{rISC}}$ **($\times 10^6$ s^{-1})**	k_{FI} ($\times 10^7$ s^{-1})	$\boldsymbol{k_{rISC}}$ **($\times 10^6$ s^{-1})**
PXZ-PYR	0.64	6.3	1.8	**1.8**	7.5	**1.8**
PXZ-muPYR	0.81	13.0	4.2	**6.5**	6.1	**7.2**
PXZ-mdPYR	0.63	2.5	1.7	**0.7**	4.0	**0.7**
PXZ-2mPYR	0.81	4.8	4.3	**2.5**	4.2	**2.7**

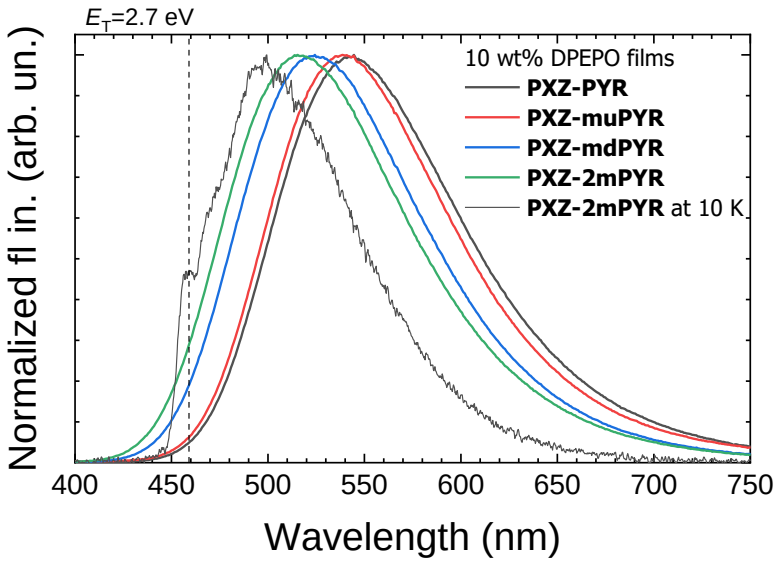

Figure S30 Emission spectra of 10wt% DPEPO films of compounds **PXZ-PYR**, **PXZ-muPYR**, **PXZ-mdPYR** and **PXZ-2mPYR** at room temperature. 10 K phosphorescence spectrum of **PXZ-2mPYR** is also shown (dark grey line). ΔE_{ST} of nearly 0 was estimated for **PXZ-PYR** and **PXZ-muPYR**, respectively, while for **PTZ-mdPYR** and **PTZ-2mPYR** ΔE_{ST} of 50 and 100 meV was estimated, respectively.

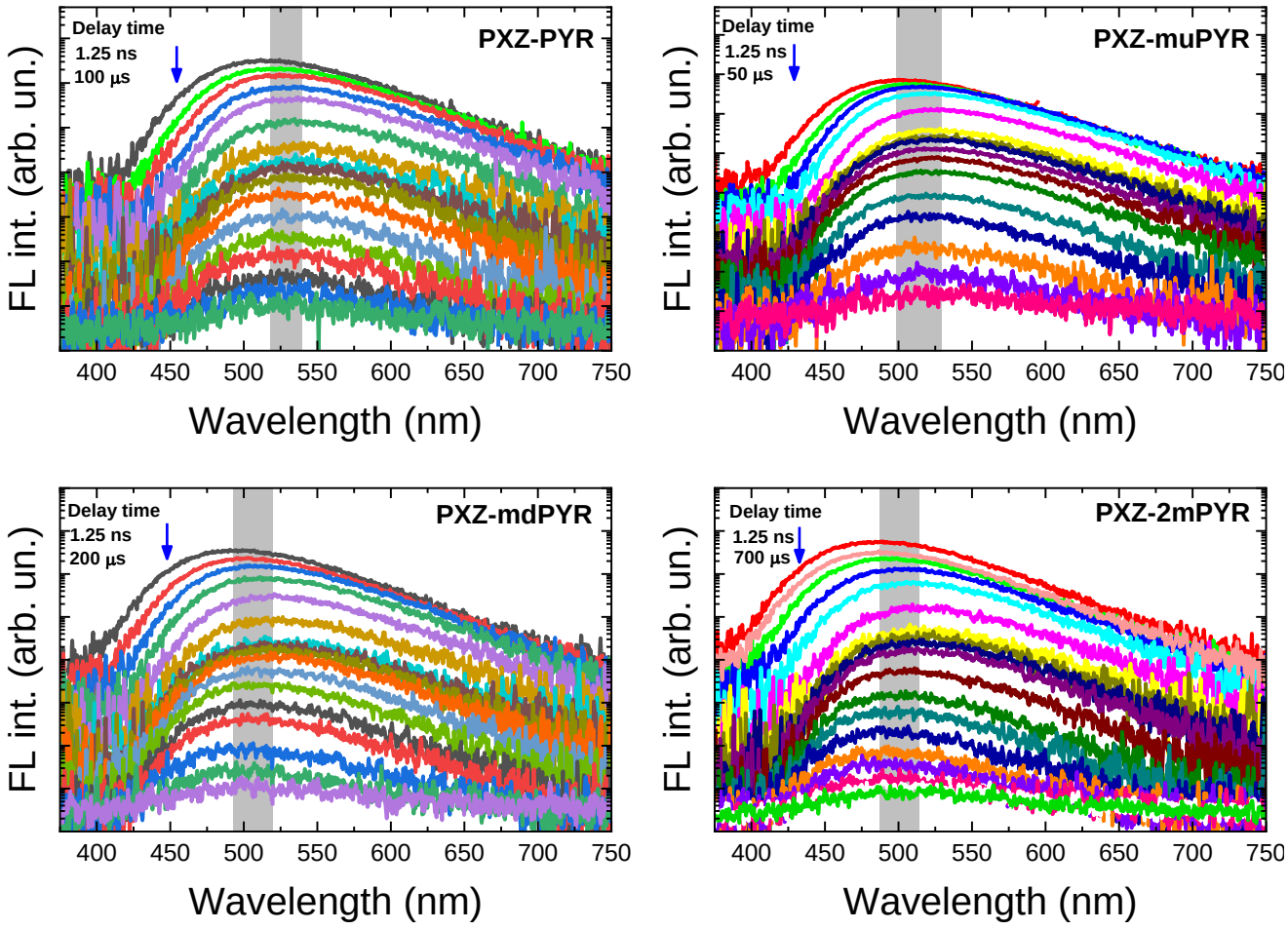

Figure S31 Time-resolved fluorescence spectra of 10wt% DPEPO films of compounds **PXZ-PYR**, **PXZ-muPYR**, **PXZ-mdPYR** and **PXZ-2mPYR** at room temperature in $-O_2$ conditions. Shaded area shows the spectral range where temporal shifts of emission peak occours.

Table S2. Several examples of TADF compounds with short solid-state TADF lifetime.

Name	λ_{Fl} (nm)	τ_{TADF} (μs)	peak EQE (%)	Reference
5c	around 540	1.4	-	[13]
5e	around 540	1.0	-	[13]
PTZ-PN	around 570	1.1	0.58	[14]
DHPZ-2BTZ	around 576	1.0	5	[15]
DTC-mBPSB	434	1.16	5.5	[16]
DMTDAc	around 450	1.2	19.8	[17]
DCzIPN	447	1.2	16.4	[18]
TB-3PXZ	509	1.3	13.9	[19]
DPXZ-as-TAZ	553	0.98	9.6	[20]
TPXZ-as-TAZ	555	1.1	13.0	[20]
PPZ-DPS	580	1.0	around 5	[21]
DCBPy	488	0.6	24.0	[22]
DTCBPy	514	1.0	27.2	[22]
PhCzDSO2	500	0.5	4.0	[23]
CzPHDSO2	523	1.1	9.1	[23]
Cz-AQ	601	0.28	5.8	[24]
TPA-AQ	622	0.37	7.5	[24]
ClPPM	547	1.39	25.3	[25]
BrPPm	546	1.32	23.6	[25]

Table S3. List of fluorescence wavelengths (λ_{FI}), fluorescence quantum yields (PLQY), TADF lifetimes (τ_{TADF}) and OLED peak EQEs of various highly efficient pyrimidine TADF compounds.

Name	λ_{FI} (nm)	PLQY	τ_{TADF} (μs)	peak EQE (%)	Reference
Acridine - pyrimidine TADF compounds					
Ac-HPM	498[b]	0.77[b]	21.4[b]	20.9	[26]
Ac-PPM	498[b]	0.79	20.7[b]	19.0	[26]
Ac-MPM	489[b]	0.80[b]	26.2[b]	20.4/24.5	[26]
Ac-NPM	480	0.63[b]	78.6[b]	14.4	[27]
Ac-1MHPM	481[b]	0.75[b]	50.3[b]	24	[28]
Ac-2MHPM	477[b]	0.71[b]	44.0[b]	20	[28]
Ac-3MHPM	454[b]	0.47[b]	45.2[b]	18	[28]
2DPAc-PPM	462[b]	0.92[b]	210[b]	20.8	[29]
2DPAc-MPM	458[b]	0.94[b]	330[b]	19.0	[29]
2SPAc-PPM	464[a]	0.97[b]	56.94[b]	31.45	[30]
DPAc-4PyPM	486[b]	0.86	22.68[b]	24.34	[31]
MFAc-PPM	464[b]	0.87[b]	38	20.4	[32]
Pm2	526[b]	0.56[a]	11.6	31.3	[33]
Pm5	541[b]	0.56[a]	5.2[b]	30.6	[33]
CzAc-26DPPM	488[b]	0.81[b]	55[b]	23.7	[34]
PM-SBA	471[b]	0.73[b]	23.1	29.2	[35]
23AcCz-PM	516[b]	0.95[b]	3.4[b]	28.4	[36]
3NPMAF	486	0.86[b]	1.7[b]	24.9	[37]
Ac-bpm	471[b]	0.75[d]	37.5[d]	17.1	[38]
55bpmAc	466[b]	0.99[d]	21.8[d]	24.9	[39]
Carbazole-pyrimidine TADF compounds					
J1	503[b]	0.67	2.2	22.0	[40]
4PyCNBCz	~480 (THF)	0.83	12.8[b]	19.8	[41]
pDTCz-DPzS	~520[b]	0.68	108[b]	18.0	[42]
Phenoxazine – pyrimidine TADF compounds					
PXZPM	535[a]	0.88[b]	2.56[b]	19.9	[3]
PXZmePM	524[a]	0.89[b]	2.11[b]	22.2	[3]
PXZPhPM■	528[a]	0.91[b]	1.99[b]	24.6	[3]
PXZ-PPM■	537[a]	0.78/0.84[c]	9.2[b]	23.7/25.1[c]	[27]
ClPPM	547	0.93[b]	1.39[b]	25.3	[25]
BrPPM	546	0.91[b]	1.32[b]	23.6	[25]
Px-bpm	524[b]	0.38[d]	25.0[d]	14.4	[38]

[a] – measured in toluene;

[b] – measured in solid-state

[c] – measured doped in CBP/DPEPO hosts;

[d] – not specified;

■ - **PXZPhPM** and **PXZ-PPM** are the same compounds.

References

(1) Kitamoto, Y.; Namikawa, T.; Ikemizu, D.; Miyata, Y.; Suzuki, T.; Kita, H.; Sato, T.; Oi, S. Light Blue and Green Thermally Activated Delayed Fluorescence from 10H-Phenoxaborin-Derivatives and Their Application to Organic Light-Emitting Diodes. *J. Mater. Chem. C* **2015**, *3* (35), 9122–9130. https://doi.org/10.1039/C5TC01380A.

(2) Xu, C.; Dong, Y.; Li, W.; Zhao, R.; Dai, Y.; Zhang, C.; Song, Q. The Role of Distance between Donor and Acceptor in Configuration Stability of Z/E Isomers Based on Cyanostilbene. *Journal of Photochemistry and Photobiology A: Chemistry* **2019**, *377*, 67–74. https://doi.org/10.1016/j.jphotochem.2019.03.035.

(3) Wu, K.; Zhang, T.; Zhan, L.; Zhong, C.; Gong, S.; Jiang, N.; Lu, Z.-H.; Yang, C. Optimizing Optoelectronic Properties of Pyrimidine-Based TADF Emitters by Changing the Substituent for Organic Light-Emitting Diodes with External Quantum Efficiency Close to 25 % and Slow Efficiency Roll-Off. *Chemistry - A European Journal* **2016**, *22* (31), 10860–10866. https://doi.org/10.1002/chem.201601686.

(4) Serevičius, T.; Skaisgiris, R.; Dodonova, J.; Jagintavičius, L.; Bucevičius, J.; Kazlauskas, K.; Jursenas, S.; Tumkevicius, S. Emission Wavelength Dependence on RISC Rate in TADF Compounds with Large Conformational Disorder. *Chemical Communications* **2019**, 55 (13), 1975-1978. https://doi.org/10.1039/C8CC08906J.

(5) Kukhta, N. A.; Batsanov, A. S.; Bryce, M. R.; Monkman, A. P. Importance of Chromophore Rigidity on the Efficiency of Blue Thermally Activated Delayed Fluorescence Emitters. *J. Phys. Chem. C* **2018**, *122* (50), 28564–28575. https://doi.org/10.1021/acs.jpcc.8b10867.

(6) Higginbotham, H. F.; Yi, C.-L.; Monkman, A. P.; Wong, K.-T. Effects of Ortho-Phenyl Substitution on the RISC Rate of D–A Type TADF Molecules. *The Journal of Physical Chemistry C* **2018**, *122* (14), 7627–7634. https://doi.org/10.1021/acs.jpcc.8b01579.

(7) Wang, K.; Zheng, C.-J.; Liu, W.; Liang, K.; Shi, Y.-Z.; Tao, S.-L.; Lee, C.-S.; Ou, X.-M.; Zhang, X.-H. Avoiding Energy Loss on TADF Emitters: Controlling the Dual Conformations of D-A Structure Molecules Based on the Pseudoplanar Segments. *Advanced Materials* **2017**, *29* (47), 1701476. https://doi.org/10.1002/adma.201701476.

(8) Chen, D.-G.; Lin, T.-C.; Chen, C.-L.; Chen, Y.-T.; Chen, Y.-A.; Lee, G.-H.; Chou, P.-T.; Liao, C.-W.; Chiu, P.-C.; Chang, C.-H.; Lien, Y.-J, Chi, Y. Optically Triggered Planarization of Boryl-Substituted Phenoxazine: Another Horizon of TADF Molecules and High-Performance OLEDs. *ACS Appl. Mater. Interfaces* **2018**, *10* (15), 12886–12896. https://doi.org/10.1021/acsami.8b00053.

(9) Etherington, M. K.; Franchello, F.; Gibson, J.; Northey, T.; Santos, J.; Ward, J. S.; Higginbotham, H. F.; Data, P.; Kurowska, A.; Dos Santos, P. L.; Graves, D.R., Batsanov A. S., Dias, F. B., Bryce M. R., Penfold Th. J., Monkman, A. P. Regio- and Conformational Isomerization Critical to Design of Efficient Thermally-Activated Delayed Fluorescence Emitters. *Nature Communications* **2017**, *8*, 14987. https://doi.org/10.1038/ncomms14987.

(10) Serevičius, T.; Bučiūnas, T.; Bucevičius, J.; Dodonova, J.; Tumkevičius, S.; Kazlauskas, K.; Juršėnas, S. Room Temperature Phosphorescence *vs.* Thermally Activated Delayed Fluorescence in Carbazole–Pyrimidine Cored Compounds. *Journal of Materials Chemistry C* **2018**, *6* (41), 11128–11136. https://doi.org/10.1039/C8TC02554A.

(11) Dias, F. B.; Penfold, T. J.; Monkman, A. P. Photophysics of Thermally Activated Delayed Fluorescence Molecules. *Methods and Applications in Fluorescence* **2017**, *5* (1), 012001. https://doi.org/10.1088/2050-6120/aa537e.

(12) Wada, Yoshimasa; Nakagawa, H.; Matsumoto, S.; Wakisaka, Y.; Kaji, H. *Molecular Design Realizing Very Fast Reverse Intersystem Crossing in Purely Organic Emitter*. 2019, ChemRxiv: doi.org/10.26434/chemrxiv.9745289.v1 ChemRxiv.org e-Print archive preprint. https://chemrxiv.org/articles/Molecular_Design_Realizing_Very_Fast_Reverse_Intersystem_Crossing_in_Purely_Organic_Emitter/9745289/1 (accessed Nov. 21, 2019).

(13) Kretzschmar, A.; Patze, C.; Schwaebel, S. T.; Bunz, U. H. F. Development of Thermally Activated Delayed Fluorescence Materials with Shortened Emissive Lifetimes. *The Journal of Organic Chemistry* **2015**, *80* (18), 9126–9131. https://doi.org/10.1021/acs.joc.5b01496.

(14) Zhang, Y.; Zhang, D.; Cai, M.; Li, Y.; Zhang, D.; Qiu, Y.; Duan, L. Towards Highly Efficient Red Thermally Activated Delayed Fluorescence Materials by the Control of Intra-Molecular $\pi - \pi$ Stacking Interactions. *Nanotechnology* **2016**, *27* (9), 094001. https://doi.org/10.1088/0957-4484/27/9/094001.

(15) Lee, J.; Shizu, K.; Tanaka, H.; Nakanotani, H.; Yasuda, T.; Kaji, H.; Adachi, C. Controlled Emission Colors and Singlet–Triplet Energy Gaps of Dihydrophenazine-Based Thermally Activated Delayed Fluorescence Emitters. *J. Mater. Chem. C* **2015**, *3* (10), 2175–2181. https://doi.org/10.1039/C4TC02530J.

(16) Liu, M.; Seino, Y.; Chen, D.; Inomata, S.; Su, S.-J.; Sasabe, H.; Kido, J. Blue Thermally Activated Delayed Fluorescence Materials Based on Bis(Phenylsulfonyl)Benzene Derivatives. *Chem. Commun.* **2015**, *51* (91), 16353–16356. https://doi.org/10.1039/C5CC05435D.

(17) Lee, I.; Lee, J. Y. Molecular Design of Deep Blue Fluorescent Emitters with 20% External Quantum Efficiency and Narrow Emission Spectrum. *Organic Electronics* **2016**, *29*, 160–164. https://doi.org/10.1016/j.orgel.2015.12.001.

(18) Cho, Y. J.; Yook, K. S.; Lee, J. Y. Cool and Warm Hybrid White Organic Light-Emitting Diode with Blue Delayed Fluorescent Emitter Both as Blue Emitter and Triplet Host. *Sci Rep* **2015**, *5* (1), 7859. https://doi.org/10.1038/srep07859.

(19) Liu, Y.; Huang, H.; Zhou, T.; Wu, K.; Zhu, M.; Yu, J.; Xie, G.; Yang, C. Boosting Photoluminescence Quantum Yields of Triarylboron/Phenoxazine Hybrids *via* Incorporation of Cyano Groups and Their Applications as TADF Emitters for High-Performance Solution-Processed OLEDs. *J. Mater. Chem. C* **2019**, *7* (16), 4778–4783. https://doi.org/10.1039/C9TC00538B.

(20) Xiang, Y.; Gong, S.; Zhao, Y.; Yin, X.; Luo, J.; Wu, K.; Lu, Z.-H.; Yang, C. Asymmetric-Triazine-Cored Triads as Thermally Activated Delayed Fluorescence Emitters for High-Efficiency Yellow OLEDs with Slow Efficiency Roll-Off. *J. Mater. Chem. C* **2016**, *4* (42), 9998–10004. https://doi.org/10.1039/C6TC02702D.

(21) Zhang, Q.; Li, B.; Huang, S.; Nomura, H.; Tanaka, H.; Adachi, C. Efficient Blue Organic Light-Emitting Diodes Employing Thermally Activated Delayed Fluorescence. *Nature Photonics* **2014**, *8* (4), 326–332. https://doi.org/10.1038/nphoton.2014.12.

(22) Rajamalli, P.; Senthilkumar, N.; Gandeepan, P.; Huang, P.-Y.; Huang, M.-J.; Ren-Wu, C.-Z.; Yang, C.-Y.; Chiu, M.-J.; Chu, L.-K.; Lin, H.-W., Cheng, Ch. H. A New Molecular Design Based on Thermally Activated Delayed Fluorescence for Highly Efficient Organic Light Emitting Diodes. *J. Am. Chem. Soc.* **2016**, *138* (2), 628–634. https://doi.org/10.1021/jacs.5b10950.

(23) Sun, K.; Sun, Y.; Jiang, W.; Huang, S.; Tian, W.; Sun, Y. Highly Efficient and Color Tunable Thermally Activated Delayed Fluorescent Emitters and Their Applications for the Solution-Processed OLEDs. *Dyes and Pigments* **2017**, *139*, 326–333. https://doi.org/10.1016/j.dyepig.2016.12.037.

(24) Huang, B.; Ji, Y.; Li, Z.; Zhou, N.; Jiang, W.; Feng, Y.; Lin, B.; Sun, Y. Simple Aggregation–Induced Delayed Fluorescence Materials Based on Anthraquinone Derivatives for Highly Efficient Solution–Processed Red OLEDs. *Journal of Luminescence* **2017**, *187*, 414–420. https://doi.org/10.1016/j.jlumin.2017.03.038.
(25) Xiang, Y.; Zhao, Y.; Xu, N.; Gong, S.; Ni, F.; Wu, K.; Luo, J.; Xie, G.; Lu, Z.-H.; Yang, C. Halogen-Induced Internal Heavy-Atom Effect Shortening the Emissive Lifetime and Improving the Fluorescence Efficiency of Thermally Activated Delayed Fluorescence Emitters. *Journal of Materials Chemistry C* **2017**, *5* (46), 12204–12210. https://doi.org/10.1039/C7TC04181K.
(26) Komatsu, R.; Sasabe, H.; Seino, Y.; Nakao, K.; Kido, J. Light-Blue Thermally Activated Delayed Fluorescent Emitters Realizing a High External Quantum Efficiency of 25% and Unprecedented Low Drive Voltages in OLEDs. *Journal of Materials Chemistry C* **2016**, *4* (12), 2274–2278. https://doi.org/10.1039/C5TC04057D.
(27) Komatsu, R.; Sasabe, H.; Nakao, K.; Hayasaka, Y.; Ohsawa, T.; Kido, J. Unlocking the Potential of Pyrimidine Conjugate Emitters to Realize High-Performance Organic Light-Emitting Devices. *Advanced Optical Materials* **2017**, *5* (2), 1600675. https://doi.org/10.1002/adom.201600675.
(28) Komatsu, R.; Ohsawa, T.; Sasabe, H.; Nakao, K.; Hayasaka, Y.; Kido, J. Manipulating the Electronic Excited State Energies of Pyrimidine-Based Thermally Activated Delayed Fluorescence Emitters To Realize Efficient Deep-Blue Emission. *ACS Applied Materials & Interfaces* **2017**, *9* (5), 4742–4749. https://doi.org/10.1021/acsami.6b13482.
(29) Park, I. S.; Lee, J.; Yasuda, T. High-Performance Blue Organic Light-Emitting Diodes with 20% External Electroluminescence Quantum Efficiency Based on Pyrimidine-Containing Thermally Activated Delayed Fluorescence Emitters. *Journal of Materials Chemistry C* **2016**, *4* (34), 7911–7916. https://doi.org/10.1039/C6TC02027E.
(30) Li, B.; Li, Z.; Hu, T.; Zhang, Y.; Wang, Y.; Yi, Y.; Guo, F.; Zhao, L. Highly Efficient Blue Organic Light-Emitting Diodes from Pyrimidine-Based Thermally Activated Delayed Fluorescence Emitters. *Journal of Materials Chemistry C* **2018**, *6* (9), 2351–2359. https://doi.org/10.1039/C7TC05746F.
(31) Zhang, Q.; Sun, S.; Lv, X.; Liu, W.; Zeng, H.; Guo, R.; Ye, S.; Leng, P.; Xiang, S.; Wang, L. Manipulating the Positions of CH···N in Acceptors of Pyrimidine–Pyridine Hybrids for Highly Efficient Sky-Blue Thermally Activated Delayed Fluorescent OLEDs. *Mater. Chem. Front.* **2018**, *2* (11), 2054–2062. https://doi.org/10.1039/C8QM00382C.
(32) Park, I. S.; Komiyama, H.; Yasuda, T. Pyrimidine-Based Twisted Donor–Acceptor Delayed Fluorescence Molecules: A New Universal Platform for Highly Efficient Blue Electroluminescence. *Chemical Science* **2017**, *8* (2), 953–960. https://doi.org/10.1039/C6SC03793C.
(33) Pan, K.-C.; Li, S.-W.; Ho, Y.-Y.; Shiu, Y.-J.; Tsai, W.-L.; Jiao, M.; Lee, W.-K.; Wu, C.-C.; Chung, C.-L.; Chatterjee, T.; Li, Y. S.; Wong., K. T. Efficient and Tunable Thermally Activated Delayed Fluorescence Emitters Having Orientation-Adjustable CN-Substituted Pyridine and Pyrimidine Acceptor Units. *Adv. Funct. Mater.* **2016**, *26* (42), 7560–7571. https://doi.org/10.1002/adfm.201602501.
(34) Nakao, K.; Sasabe, H.; Komatsu, R.; Hayasaka, Y.; Ohsawa, T.; Kido, J. Significant Enhancement of Blue OLED Performances through Molecular Engineering of Pyrimidine-Based Emitter. *Advanced Optical Materials* **2017**, *5* (6), 1600843. https://doi.org/10.1002/adom.201600843.
(35) Liu, M.; Komatsu, R.; Cai, X.; Hotta, K.; Sato, S.; Liu, K.; Chen, D.; Kato, Y.; Sasabe, H.; Ohisa, S.; Suzuri Y.; Yokoyama D.; Su Sh. J.; Kido, J. Horizontally Orientated Sticklike Emitters:

Enhancement of Intrinsic Out-Coupling Factor and Electroluminescence Performance. *Chem. Mater.* **2017**, *29* (20), 8630–8636. https://doi.org/10.1021/acs.chemmater.7b02403.

(36) Zhang, Q.; Sun, S.; Chung, W. J.; Yoon, S. J.; Wang, Y.; Guo, R.; Ye, S.; Lee, J. Y.; Wang, L. Highly Efficient TADF OLEDs with Low Efficiency Roll-off Based on Novel Acridine–Carbazole Hybrid Donor-Substituted Pyrimidine Derivatives. *J. Mater. Chem. C* **2019**, *7* (39), 12248–12255. https://doi.org/10.1039/C9TC04284A.

(37) Ganesan, P.; Chen, D.-G.; Liao, J.-L.; Li, W.-C.; Lai, Y.-N.; Luo, D.; Chang, C.-H.; Ko, C.-L.; Hung, W.-Y.; Liu, S.-W.; Lee, G. H; Chou, P. T.; Chi, Y. Isomeric Spiro-[Acridine-9,9'-Fluorene]-2,6-Dipyridylpyrimidine Based TADF Emitters: Insights into Photophysical Behaviors and OLED Performances. *J. Mater. Chem. C* **2018**, *6* (37), 10088–10100. https://doi.org/10.1039/C8TC03645D.

(38) Park, H.-J.; Han, S. H.; Lee, J. Y. Molecular Design of Thermally Activated Delayed-Fluorescent Emitters Using 2,2'-Bipyrimidine as the Acceptor in Donor-Acceptor Structures. *Chem. Asian J.* **2017**, *12* (18), 2494–2500. https://doi.org/10.1002/asia.201700889.

(39) Park, H.-J.; Han, S. H.; Lee, J. Y.; Han, H.; Kim, E.-G. Managing Orientation of Nitrogens in Bipyrimidine-Based Thermally Activated Delayed Fluorescent Emitters To Suppress Nonradiative Mechanisms. *Chem. Mater.* **2018**, *30* (10), 3215–3222. https://doi.org/10.1021/acs.chemmater.8b00006.

(40) Gómez-Bombarelli, R.; Aguilera-Iparraguirre, J.; Hirzel, T. D.; Duvenaud, D.; Maclaurin, D.; Blood-Forsythe, M. A.; Chae, H. S.; Einzinger, M.; Ha, D.-G.; Wu, T.; Markopoulos, G.; Jeon S.; Kang, H.; Miyazaki H.; Numata M.; Kim., S.; Huang, W.; Hong, S. I; Baldo, M.; Adams, R. P.; Aspuru-Guzik, A. Design of Efficient Molecular Organic Light-Emitting Diodes by a High-Throughput Virtual Screening and Experimental Approach. *Nature Materials* **2016**, *15* (10), 1120–1127. https://doi.org/10.1038/nmat4717.

(41) Jang, J. S.; Lee, H. L.; Lee, K. H.; Lee, J. Y. Electrostatic Potential Dispersing Pyrimidine-5-Carbonitrile Acceptor for High Efficiency and Long Lifetime Thermally Activated Delayed Fluorescence Organic Light-Emitting Diodes. *J. Mater. Chem. C* **2019**, *7* (40), 12695–12703. https://doi.org/10.1039/C9TC04304G.

(42) Wang, L.; Cai, X.; Li, B.; Li, M.; Wang, Z.; Gan, L.; Qiao, Z.; Xie, W.; Liang, Q.; Zheng, N.; Liu, K.; Su, Sh-J. Achieving Enhanced Thermally Activated Delayed Fluorescence Rates and Shortened Exciton Lifetimes by Constructing Intramolecular Hydrogen Bonding Channels. *ACS Appl. Mater. Interfaces* **2019**, *11* (49), 45999-46007. https://doi.org/10.1021/acsami.9b16073.